

The Computational Capacity of LRC, Memristive and Hybrid Reservoirs

Forrest C. Sheldon,^{1,*} Artemy Kolchinsky,² and Francesco Caravelli¹

¹*Theoretical Division and Center for Nonlinear Studies,*

Los Alamos National Laboratory, Los Alamos, New Mexico 87545, USA

²*Santa Fe Institute, 1399 Hyde Park Road, Santa Fe, NM 87501, USA*

Reservoir computing is a machine learning paradigm that uses a high-dimensional dynamical system, or *reservoir*, to approximate and predict time series data. The scale, speed and power usage of reservoir computers could be enhanced by constructing reservoirs out of electronic circuits, and several experimental studies have demonstrated promise in this direction. However, designing quality reservoirs requires a precise understanding of how such circuits process and store information. We analyze the feasibility and optimal design of electronic reservoirs that include both linear elements (resistors, inductors, and capacitors) and nonlinear memory elements called memristors. We provide analytic results regarding the feasibility of these reservoirs, and give a systematic characterization of their computational properties by examining the types of input-output relationships that they can approximate. This allows us to design reservoirs with optimal properties. By introducing measures of the total linear and nonlinear computational capacities of the reservoir, we are able to design electronic circuits whose total computational capacity scales extensively with the system size. Our electronic reservoirs can match or exceed the performance of conventional “echo state network” reservoirs in a form that may be directly implemented in hardware.

PACS numbers: 05.45.Tp, 05.90.+m, 07.50.Ek

Keywords: Memory circuits | Reservoir Computing | Memory Capacity | Memory-Nonlinearity tradeoff

I. INTRODUCTION

Reservoir computing (RC) [16, 17, 20] is a model for performing computations on time series data, which combines a high-dimensional driven dynamical system, called a *reservoir*, with a simple learning algorithm. Reservoir computing has proven to be a powerful tool in a wide variety of signal processing tasks, including forecasting [16], pattern generation and classification [4], adaptive filtering and prediction of chaotic systems [18]. Recently, extensions to spatio-temporal chaotic systems [26] have proven to be surprisingly effective.

Central to the success of reservoir computation is the use of large dynamical systems to generate nonlinear transformations and store memories of the driving signal. This has generated interest in developing nanoscale electronic reservoirs with large numbers of elements [28], incorporating both linear components (such as resistors, inductors, and capacitors) and nonlinear components such as *memristors*. Memristors, or “resistors with memory”, are nanoscale devices whose resistance depends on the past history of the current. The currents flowing through these devices cause a rearrangement of ions, leading to a persistent (but also reversible) change in resistance. Memristors offer the possibility of harnessing both nonlinear behavior and memory in electronic circuits. For this reason, specialized circuits composed of large numbers of memristors promise a new generation of computational hardware operating orders of magnitude faster, and at far lower power, than traditional digital circuitry [1, 6, 10, 27, 29, 32].

Recently, several experimental works examining memristor-based electronic reservoirs have shown remarkable promise

[3, 9, 12, 15, 19, 23, 25]. However, there is still no fundamental understanding of when electronic circuits can be successfully employed as reservoirs, what type of functions they can compute, and how to design electronic reservoirs with specific computational properties. In this paper we address this gap by providing a systematic and analytical study of the computational capacity of electronic reservoirs composed of traditional linear elements and memristors.

In order to be feasible as a reservoir, a driven dynamical system must satisfy certain properties which guarantee that its state encodes an informative function of the driving signal; we establish feasibility for models of linear/LRC (inductor-resistor-capacitor) and memristor reservoirs. We also characterize the input-output relationships natural to electronic reservoirs, in the process showing how memristors may be viewed as a source of nonlinear computations. We then demonstrate how to combine linear and nonlinear elements to achieve a specific computational task (that of approximating a 2nd order filter). Lastly, the capacity of the reservoir to perform useful computations should increase as the size (i.e., dimensionality) of the reservoir is increased. In particular, the main motivation for electronic reservoirs is the potential to achieve very large reservoir sizes, but increases in size are useless if they do not lead to improved computational capacities of the reservoir. Optimally, the number of linearly independent inputs that the reservoir can reconstruct should scale linearly with the reservoir size — i.e., to borrow a term from statistical physics, their reconstruction capabilities should be extensive in reservoir size. For both LRC and memristor reservoirs, we consider measures of linear and nonlinear computational capacity, and show that they can be made to scale extensively. The approach we use to analyze the computational capacities of memristor and LRC reservoirs may be generalized to other reservoirs and computational tasks in analogy to the methods available to tune echo state networks (ESNs) by trading between memory

* To whom correspondence should be addressed. E-mail: fs@lms.ac.uk;
Current Address: London Institute for Mathematical Sciences, 21 Albermarle St. London, W1S 4BS, UK

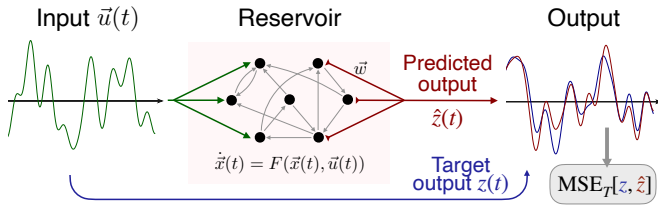


Figure 1. Basics of reservoir computing. A time-dependent input $\vec{u}(t)$ is used to drive a reservoir, which is a (linear or nonlinear) dynamical system with internal state $\vec{x}(t)$. The predicted output is computed as a weighted linear combination of the internal state, $\hat{z}(t) = \vec{w}^T \vec{x}(t)$. The weights \vec{w} are adjusted to minimize the time-averaged mean squared error (MSE) between this predicted output and the target output $\vec{z}(t)$.

storage and nonlinearity.

In the next section we make these notions more precise. We provide an introduction to reservoir computing, electronic reservoirs and memristors, as well as definitions of the measures of computational capacity we will utilize. We then turn to the feasibility, tunability and scalability of LRC and memristor-based reservoirs. Finally, we compare our results to more conventional ESN reservoirs [16], showing that electronic reservoirs are capable of matching or exceeding the performance of a standard ESN reservoir implementations.

BACKGROUND

Reservoir Computing

In what follows, we present a brief review of reservoir computing in continuous time. A schematic illustration is provided in fig. 1. Readers familiar with RC and measures of capacity may skip to the section labelled Circuit Elements and Structure.

A *reservoir* is a multivariate driven dynamical system. At time t , the state of the dynamical system, which we indicate as $\vec{x}(t)$, is driven by an input $\vec{u}(t)$ and obeys the differential equation

$$\dot{\vec{x}}(t) = F(\vec{x}(t), \vec{u}(t)). \quad (1)$$

As a result of these dynamics, the state of the reservoir encodes information about \vec{u} as transformations of its previous history. As an instructive example, a linear reservoir is governed by the equation

$$\dot{\vec{x}}(t) = A\vec{x}(t) + \vec{u}(t). \quad (2)$$

which has the long time limit solution

$$\vec{x}(t) = \int_0^\infty d\tau e^{A\tau} \vec{u}(t - \tau) \quad (3)$$

showing that the state is a linear function of the past history of \vec{u} . We will consider reservoirs driven by a scalar input signal $u(t)$ as $\vec{u}(t) = \vec{v}u(t)$, where \vec{v} is a vector of weights

that defines how the input signal $u(t)$ enters into each element of the reservoir.

In order for a dynamical system to be considered *feasible* as a reservoir, its state must approach a nontrivial function of the input trajectory in the long time limit. At a high level, we can state this requirement in terms of two conditions:

- *Fading Memory*: If the system were to be started from two different initial conditions $\vec{x}_0, \neq \vec{x}'_0$ and driven with the same input trajectory u , the system's trajectories should eventually converge to the same state, $\vec{x}(t), \vec{x}'(t) \rightarrow \vec{x}[u](t)$ as $t \rightarrow \infty$. The statement above implies that the system has a finite temporal memory.
- *State Separation*: Different input sequences should drive the system into different trajectories, i.e., if the same initial condition were to be driven with two different input trajectories $u \neq u'$, the resulting reservoir trajectories must be sufficiently different.

The first condition requires that the state of the reservoir becomes a function of the input trajectory, while the second requires that the this function carries information about the input trajectory.

Reservoirs that satisfy the fading memory property have a representation as a Wiener/Volterra series [5],

$$x_i[u](t) = \int_0^\infty d\tau_1 h_{i1}(\tau_1)u(t - \tau_1) + \int_0^\infty d\tau_1 d\tau_2 h_{i2}(\tau_1, \tau_2)u(t - \tau_1)u(t - \tau_2) + \dots \quad (4)$$

which decomposes each degree of freedom x_i into a series of linear and nonlinear components governed by kernel functions $h_{in}(\tau_1, \dots, \tau_n)$. This allows us to regard the reservoir as implementing a *filter* of the input trajectory. Reservoir computers can be thought of as approximating filters, in much the same that feed-forward neural networks may be thought of as approximating functions [21, 22]. This will be a useful characterization of both the reservoir and its possible outputs.

In addition to the input trajectory $u(t)$, we are also provided with a target output trajectory $z(t)$. The goal of reservoir computing is to learn to approximate the input-output mapping $u \mapsto z$ with an estimate $\hat{z}(t)$, which is a linear combination of the reservoir's variables, $\hat{z}(t) = \vec{w}^T \vec{x}(t)$. Here we will always assume that the $z(t)$ is a scalar. We will also assume that the target output is a function of u of the form in eqn. (4), denoted as $z[u]$. See fig. 1 for details. Finally, as is often done, to the reservoir trajectories \vec{x} we append a constant signal, $\vec{x}'(t) := [\vec{x}(t), \vec{1}(t)]$ to compensate for constant shifts in the output $z[u]$.

In the following, all quantities depend on the particular input signal $u = \{u(t) : 0 \leq t \leq T\}$ used to drive the reservoir and generate $\vec{x}[u](t)$, $\hat{z}[u](t)$, and $z[u](t)$. This dependence on u can be cumbersome to denote and so we have suppressed it in favor of indicating the dependence on the time interval by the subscript \square_T .

The interesting feature of RC is that only the output layer, given by the coefficients \vec{w} , is trained. Training is performed

in the following manner: First, the reservoir is “initialized” by driving with the input signal on an interval $[-T', 0]$, until the fading memory property ensures that its state is independent of the initial condition at $t = -T'$. Then, reservoir is driven for an additional interval $[0, T]$. The coefficients \vec{w} are learned via linear regression, by minimizing the time-averaged mean squared error (MSE) between a reconstruction $\hat{z}(t) = \vec{w}^T \vec{x}'(t)$ and the target output trajectory $z(t)$ over the time interval $[0, T]$,

$$\text{MSE}_T[z, \hat{z}] = \frac{1}{T} \int_0^T dt (z(t) - \hat{z}(t))^2. \quad (5)$$

This optimization problem $\hat{w} = \text{argmin}_{\vec{w}} \text{MSE}_T[z, \vec{w}^T \vec{x}']$ has a closed form solution (note the use of the ‘hat’ to denote the optimum). Defining the time average, $\langle f \rangle_T = \frac{1}{T} \int_0^T dt f(t)$, the solution is $\hat{w} = \langle \vec{x}'^T \vec{x}' \rangle_T^{-1} \langle \vec{x}'^T z \rangle_T$ which we show in the supplemental material. Regularization via ridge regression is also commonly employed in practice, which modifies the objective to $\text{MSE}_T[z, \vec{w}^T \vec{x}'] + k \|\vec{w}\|^2$ [20].

In the space of functions on $[0, T]$ the optimal approximation $\hat{z}(t) = \hat{w}^T \vec{x}'(t)$ can be understood as the projection of $z(t)$ onto the span of the reservoir trajectories $\vec{x}'(t)$. This is a consequence of the least squares objective [11]. As the estimate $\hat{z}(t)$ is a projection of $z(t)$, we can evaluate the normalized mean-squared error of the reservoir reconstruction of z as

$$\text{nMSE}_T[z, \hat{z}] = \frac{\text{MSE}_T[z, \hat{z}]}{\langle z^2 \rangle_T}. \quad (6)$$

It is normalized to $0 \leq \text{nMSE}_T[z] \leq 1$ when calculated on the training interval $t \in [0, T]$. The nMSE is often a more useful measure than the MSE, since it gives the *relative* error of the approximation to the variation in $z(t)$.

From now on we will only consider the optimal approximation generated by the reservoir. We introduce the notation

$$\text{nMSE}_T[z] \equiv \min_{\vec{w}} \text{nMSE}_T[z, \vec{w}^T \vec{x}]. \quad (7)$$

$\text{nMSE}_T[z]$ can be read as *the normalized mean-squared error for the reservoir’s approximation of z on the time interval $[0, T]$* . Some authors [11] prefer to use a reversed scale, defining the *capacity* of the reservoir to approximate z as

$$C_T[z] = 1 - \text{nMSE}_T[z], \quad (8)$$

where $\langle f \rangle_T = \frac{1}{T} \int_0^T dt f(t)$. The capacity is bounded $0 \leq C_T[z] \leq 1$ with 1 corresponding to a perfect reconstruction.

As mentioned above, the nMSE and capacity C_T can be given a geometric interpretation on the space of functions on $[0, T]$. For a function $z(t)$ normalized as $\langle z^2 \rangle_T = 1$, the capacity $C_T[z]$ is the squared length of the projection of z onto the span of the reservoir trajectories \vec{x}' . The $\text{nMSE}[z]$ is the squared length of the component of $z(t)$ perpendicular to the span of the reservoir trajectories and so $C_T[z] + \text{nMSE}[z] = 1$ can be seen as an expression of the Pythagorean Theorem.

Total Memory and Extensivity

In order to assess a reservoir, we require a more complete picture of its properties, that goes beyond its ability to approximate a single function. A main result of Dambre et al. [11] is that the capacities of a reservoir to approximate orthogonal functions give independent information about the reservoir (orthogonality is defined as $\lim_{T \rightarrow \infty} \langle z z' \rangle_T \rightarrow 0$, see supplemental material for further details).

One consequence of this result is that, in the long-time limit, capacities will converge to time-independent values that characterize the reservoir,

$$\lim_{T \rightarrow \infty} C_T[z] = C[z]. \quad (9)$$

While we cannot achieve this limit in practice, we can estimate it using techniques from finite size scaling. (The capacities we report throughout this paper are obtained from these techniques, with detailed results of the analysis shown in the supplemental material.)

Another consequence of the result by Dambre is that, rather than evaluating the reservoir’s capacity to approximate only a single function z , we can evaluate its capacity over a family of orthogonal functions $\{z_i\}$. The resulting capacities allow us to characterize the reservoir’s ability to approximate arbitrary functions of the form $\sum_i a_i z_i$. We relate the capacities of the reservoir on a family of functions, $C_T[z_i]$, to a linear combination of these functions, $C_T[\sum_i a_i z_i]$, in a precise way: *Consider a set of n orthonormal functions on $t \in [0, T]$, $\langle z_i z_j \rangle_T = \delta_{ij}$, and normalized linear combination $z = \sum_{i=1}^n a_i z_i$, $\langle z^2 \rangle_T = 1$. Then, if $C_T[z_i] \geq 1 - \epsilon$ for all $i = 1 \dots n$ then $C_T[z] \geq 1 - n\epsilon$. This is proved in the supplemental material, where we also construct the function z^* that has maximal error. Our construction show that when errors are uncorrelated, or when the maximal error function lies within the basis, the capacity on the linear combination satisfies the tighter bound $C_T[z^*] \geq 1 - \epsilon$.*

A natural family of functions for evaluating capacities are products of the delayed input $z(t) = u(t - \tau_1) \dots u(t - \tau_n)$, that is the terms in the Wiener/Volterra series in eqn. (4). The first two such functions are shown schematically in fig. 2. The first function, $z(t) = u(t - \tau_1)$ leads to the *linear memory function*,

$$m(\tau) = C[u(t - \tau)], \quad (10)$$

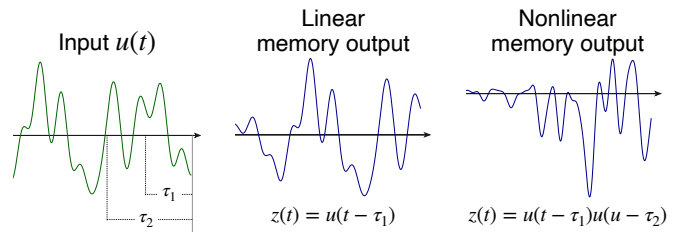


Figure 2. The first two terms of the Wiener/Volterra series, eqn. (4), are linear and quadratic functions of the input. When taken as the target output z , these functions are used to define the linear and nonlinear memory of the reservoirs, as in eqns. 10 and 11.

which reflects the ability of the reservoir to reconstruct time-delayed version of the input at different lags [14, 17, 31]. We generalize this concept to nonlinear, n^{th} -order memory functions,

$$m_n(\tau_1, \tau_2, \dots, \tau_n) = C[u(t - \tau_1)u(t - \tau_2) \dots u(t - \tau_n)], \quad (11)$$

which reflect the reservoir's ability to approximate the product of the input at various delays in the past. Achieving high nonlinear memory requires the reservoir to memorize past inputs as well as to be able to perform nonlinear operations on these inputs.

If the input function u is drawn from a family of random functions with mean zero $\langle u \rangle_T = 0$ and decaying auto-correlation $\langle u(t)u(t - \tau) \rangle_T \rightarrow 0$ as $\tau \rightarrow \infty$, then u and its time delayed products will approach orthogonality as their delays differ. We generate input functions from smoothed Gaussian noise with correlations that decay exponentially with a unit timescale (see supplemental material). The family of functions $\{u(t - \tau_1), u(t - \tau_1)u(t - \tau_2), u(t - \tau_1)u(t - \tau_2)u(t - \tau_3) \dots\}$ is approximately orthogonal for time delays satisfying $|\tau_i - \tau_j| > 1$. The memory functions m_n thus tell us independent information about the computational capacities of our reservoir over timescales greater than 1.

Finally, we summarize a reservoir's computational properties via the following quantity:

$$\tau_\epsilon = \int_0^\infty d\tau \Theta(m(\tau) > 1 - \epsilon), \quad (12)$$

where Θ is the Heaviside step function. We refer to τ_ϵ as the *total linear memory* of the reservoir. This quantity captures the time delay up to which the history of the input is reconstructed with an error less than ϵ . This definition can be generalized to quantify the *total n^{th} -order nonlinear memory* as

$$\tau_\epsilon^{(n)} = \int_0^\infty \dots \int_0^\infty d\tau_1 \dots d\tau_n \Theta(m_n(\tau_1, \dots, \tau_n) > 1 - \epsilon). \quad (13)$$

Previous studies have demonstrated linear reservoirs with extensive total memory, *i.e.* $\tau_\epsilon \propto N$ for a reservoir with N elements [14, 31]. In this work we present an electronic implementation of the linear reservoirs discussed in those papers. We then generalize this approach by designing an electronic reservoir which displays extensive scaling in its total quadratic-memory, $\tau_\epsilon^{(2)} \propto N$.

Circuit Elements and Structure

We consider electronic circuits composed of traditional linear elements including inductors (L), capacitors (C), and resistors (R), active elements (voltage or current sources), as well as passive memory elements known as memristors (Mem) (see below). In all cases, the electronic reservoir will accept a vector input through a set of voltage sources \vec{s} . We can convert the scalar input $u(t)$ to a time dependent voltage vector $\vec{s}(t)$ through a set of constant input weights $\vec{s}(t) = \vec{v}u(t)$. We will

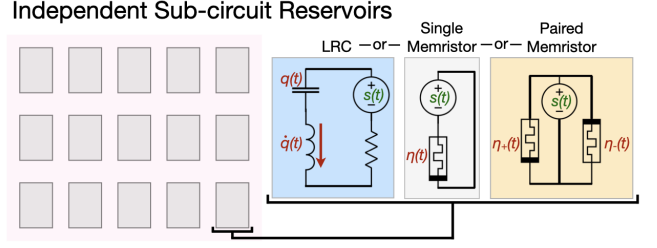


Figure 3. A class of reservoirs we consider are composed of independent sub-circuits. Each circuit has identical structure, but with parameters that vary to achieve independent trajectories when driven with the same input. In all sub-circuits the input is a voltage generator driven with $s(t)$ and shown in green. The output circuit variables are shown in red. The three sub-circuit types are: LRC circuits with output variables $q(t)$, the charge on the capacitor and $\dot{q}(t)$, the current through the inductor, single memristors with output variable $\eta(t)$, the memristive state variable, and paired memristors biased in opposite directions with output variables $\eta_+(t)$ and $\eta_-(t)$. As the resistance is a linear function of η , the two are equivalent as output variables.

consider several circuit structures as shown in figs. 3 and 4, including independent sub-circuit reservoirs composed of LRC, single and paired memristor circuits and memristive networks on a lattice.

The linear reservoirs we consider will be composed of sets of LRC sub-circuits as shown in fig. 3 in which each LRC circuit, indexed by n has component values l_n, r_n, c_n and is driven by a voltage generator $s_n = u(t)$ (taking $\vec{v} = \vec{1}$). Each circuit possesses two degrees of freedom $q_n(t), \dot{q}_n(t)$ corresponding to the charge across and current entering the capacitor, which obey the following equations of motion:

$$\begin{bmatrix} \dot{q}_n(t) \\ \dot{\ddot{q}}_n(t) \end{bmatrix} = \begin{bmatrix} 0 & 1 \\ -\frac{1}{l_n c_n} & -\frac{r_n}{l_n} \end{bmatrix} \begin{bmatrix} q_n(t) \\ \dot{q}_n(t) \end{bmatrix} + \begin{bmatrix} 0 \\ \frac{s_n(t)}{l_n} \end{bmatrix}. \quad (14)$$

The output trajectories of an LRC sub-circuit are the trajectories of the internal degrees of freedom, $\vec{x} = [\vec{q}(t), \dot{\vec{q}}(t)]$ (the vector notation covers the indexing over n). The dimension of an LRC reservoir of N sub-circuits is thus $2N$. In the supplemental information we prove that a network of LRC motifs is equivalent to a collection of separate sub-circuits. There is thus no benefit to considering a network of these motifs and our treatment here is fully general.

In addition to linear elements, we consider reservoirs of nonlinear electronic components called memristors. Memristors are passive 2-terminal devices characterized by the response relationship,

$$V(t) = R(\eta)I(t), \quad (15)$$

$$\dot{\eta}(t) = f(\eta(t), I(t)), \quad (16)$$

where $V(t)$ is the voltage drop across the memristor, $I(t)$ is current, $\eta(t)$ is the internal state of the memristor, and $R(\eta(t))$ is the state-dependent resistance. It can be seen that the resistance can depend on the past history of the current. Importantly, memristors are inherently nonlinear elements. As in the case of linear networks, the input to the circuits is through

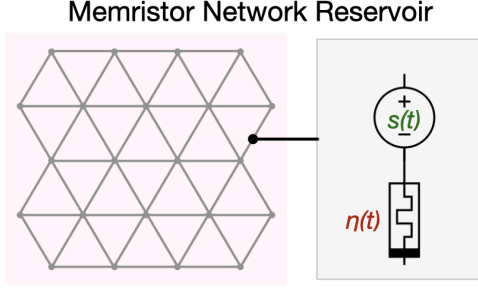


Figure 4. The edges of the memristor networks we consider consist of voltage driven memristors which are arranged in a triangular lattice. The output variables are the memristive states in the networks $\vec{\eta}(t) = [\eta_1(t), \eta_2(t), \dots]$. The magnitude of the driving signal in each edge $s_e(t)$ varies on the interval $[S, -S]$ in equally spaced increments.

a set of voltage generators $\vec{s}(t) = \vec{v}u(t)$ where \vec{v} is a constant vector of weights with units of voltage.

The internal states of a memristor circuit closely mimic the behavior of a neural network. We constrain ourselves to the linear current model similar to the one proposed in [27], along with a decay term [8],

$$R(\eta) = R_{\text{off}}(1 - \eta) + R_{\text{on}}\eta, \quad (17)$$

$$R(\eta) = R_{\text{off}}(1 - \chi\eta) \quad \left(\chi := \frac{R_{\text{off}} - R_{\text{on}}}{R_{\text{off}}} \right), \quad (18)$$

$$\dot{\eta}(t) = -\alpha\eta(t) + \frac{R_{\text{off}}}{\beta}I(t). \quad (19)$$

Here the constant $\alpha = 1/t^*$ is an inverse time scale while β is an activation current per unit of time, which moderates the strength of the input signal. This model is the simplest approximation of a current-controlled memristor, as we show in the supplementary material. The internal state η is limited to the interval $[0, 1]$ by hard barriers, so the resistance $R(\eta)$ varies between two limiting values $[R_{\text{on}}, R_{\text{off}}]$. We use η as the output variable of memristors, but as the resistance R is a linear function of η , the two are equivalent as components of a linear regression.

The term $-\alpha\eta(t)$ in eqn. (19) causes the memristor state η to decay to 0 in the absence of a current. This is called volatility in the context of memristors and is an important effect in many memory materials and their applications (see the review [30]). Here it plays a central role in providing the fading memory property for memristor circuits. However, not all memristors are volatile and commercial memristors are generally designed to be nonvolatile for memory applications. While nonvolatile memristors can still show fading memory (see [2, 24]), nonvolatile fading memory is much more difficult to treat analytically and so we limit our study to the case of volatile memristors. This is not as great a limitation as it might seem, in the sense that any nonvolatile memristor can be turned into a volatile memristor by the addition of a voltage or current source that gives a small negative current in the absence of an applied voltage.

When considering networks of elements as in fig. 4 it is convenient to introduce the cycle space projector Ω_A [8], which

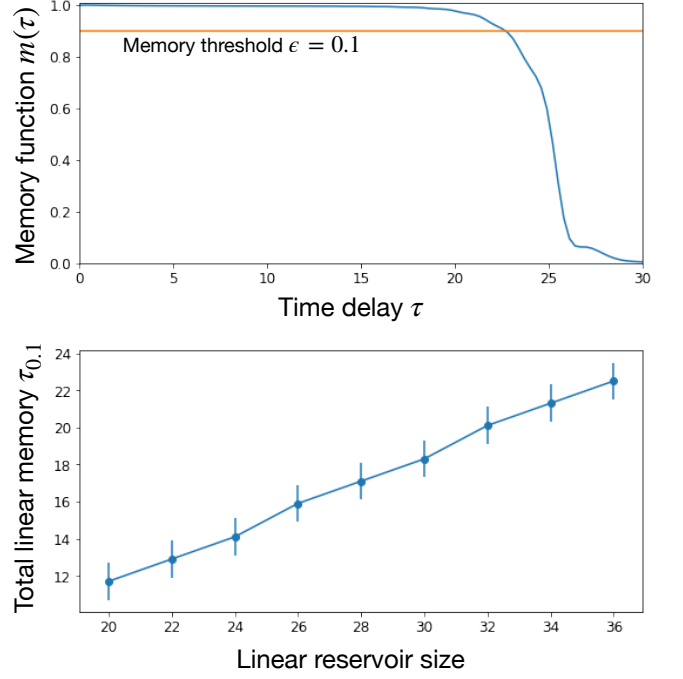


Figure 5. The top panel displays the memory function for an LRC reservoir of 18 sub-circuits (36 trajectories) with $\Delta\omega = \gamma = \frac{4}{18}$. The memory function $m(\tau)$ displays the capacity of the reservoir to reconstruct the delayed input $u(t - \tau)$. The reservoir retains an accurate memory of the input before falling sharply. In the bottom panel we display the $\epsilon = 0.1$ total linear memory of LRC networks of various sizes. This corresponds to the signal delay at which the memory function falls below 0.9, displayed in the top panel as a vertical line. As discussed in the main text, the total linear memory scales extensively with the system size.

projects a vector that assigns a real number to each edge of a graph onto current configurations that satisfy Kirchhoff's current law. The projector Ω_A can be simply computed from the circuit graph \mathcal{G} , in which nodes of the graph represent electrical junctures and edges contain electrical elements. For a circuit in which the edges contain a voltage generator in series with a memristor with values $\vec{u}(t)$, as in fig. 4, the equation of motion is given by [8]

$$\dot{\vec{\eta}}(t) = -\alpha\vec{\eta}(t) + \frac{1}{\beta}(I - \chi\Omega_A H(t))^{-1}\Omega_A\vec{u}(t) \quad (20)$$

where we have used the convention $H(t) = \text{diag } \vec{\eta}(t)$. Interactions between memristors thus occur through the inverse of $I - \chi\Omega_A H(t)$ and are mediated both by χ and the Kirchhoff laws imposed by Ω_A . A memristor circuit generates reservoir trajectories $\vec{x} = \vec{\eta}(t)$.

RESULTS

Linear Electronic Reservoirs

In this section we illustrate the ideas of memory and scaling introduced above in the familiar realm of linear circuits. We show that electronic reservoirs with extensive total memory can be constructed from LRC circuits and that these circuits can be understood as calculating a time-windowed version of the Fourier transform, akin to a spectrogram. Moreover, in the supplemental material, we prove the following result:

Feasibility of LRC circuits. *Reservoirs of LRC circuit motifs satisfy the fading memory and state separation properties.*

This justifies our use of these systems as reservoirs and the application of the memory measures defined above.

From the solution in eqn. (3), we observe that linear reservoirs generate linear functions of the input signal, and that their properties will depend on the eigenvalues of A . We thus examine the scaling of the total linear memory τ_ϵ using spectral techniques. In [14, 31], it was noted that an extensive total memory was obtained for reservoirs with eigenvalues lying on a vertical line in the negative half plane, i.e., eigenvalues of the form $\lambda_{n,\pm} = -\gamma \pm in\Delta\omega$ for $n \in \{0 \dots N\}$. As shown in the supplemental material, the solution to eqn. (14) depends on linear combinations of the integrals $\int_0^\infty d\tau e^{\lambda_{n,\pm}\tau} u(t-\tau)$. For the values of $\lambda_{n,\pm}$ above, this can be interpreted as calculating a local Fourier transform of the input. The frequencies $\text{Im}(\lambda_{n,\pm}) = \pm n\Delta\omega$ are evenly spaced with largest frequency $N\Delta\omega$ and smallest frequency $\Delta\omega$. The exponential window, $e^{-\gamma\tau}$ applies a cutoff in time on the interval $0 \leq \tau \leq 1/\gamma$. This means that in order to not experience interference with previous time windows, we should set the lowest frequency, $\Delta\omega$ to be on the same order as γ . Further details on this correspondence are given in the supplemental material (section VIII. Solution of LRC Circuits).

The LRC sub-circuit in fig. 3 and governed by eqn. (14) has eigenvalues $\lambda_\pm = -\frac{\gamma}{2l} \pm i\sqrt{\frac{1}{lc} - \frac{\gamma^2}{4l^2}} = -\gamma \pm i\omega$ and a corresponding pair of trajectories $q_n(t)$, $\dot{q}_n(t)$ corresponding to the charge and current entering the capacitor (see supplemental material). As a consequence *any eigenvalue spectrum in the negative half-plane and symmetric in the upper and lower half planes can be achieved by a collection of LRC circuits with a particular choice of the component values l_n, r_n, c_n .* Given a γ and $\Delta\omega$, we choose $l_n = 1, r_n = 2\gamma$ for all n and

$$c_n = \frac{1}{n^2\Delta\omega^2 + \gamma^2}, \quad (21)$$

in which case the resulting LRC circuits have eigenvalues $\lambda_{n,\pm} = -\gamma \pm in\Delta\omega$.

Reconstructing the input at a given time lag, $z(t) = u(t - \tau_1)$, is equivalent to constructing an approximate representation of the delta function as the linear term of eqn. (4), $h_1(\tau) = \delta(\tau_1 - \tau)$. After fitting, the learned weights w_{q_n} , $w_{\dot{q}_n}$ and w_c may be used to construct the kernel $h_1(\tau)$ of the reservoir. An example of this is given in the supplemental

material, which makes it clear that the training procedure is in fact constructing a delta function approximation.

To construct an LRC network of N circuits, we identify a maximum frequency ω_{\max} associated with our input signal and define $\Delta\omega = \omega_{\max}/N$ as the lowest frequency and resolution. This lowest frequency defines a timescale $t' \sim 1/\Delta\omega$ over which a signal could be represented by the Fourier series. We then choose $\gamma = \Delta\omega$ to suppress the signal for times longer than t' . For the smoothed Gaussian noise input signal used here (see supplemental material), we take $\omega_{\max} = 4$.

We expect that if ω_{\max} is chosen to be sufficiently large so as to accurately represent the signal, the system's total linear memory τ_ϵ will scale as N . This is confirmed in fig. 5, where we show the memory function $m(\tau) = C[u(t-\tau)]$ and the total linear memory τ_ϵ for $\epsilon = 0.1$ across a range of reservoir sizes. As expected, reservoirs of this type show an extensive total linear memory. Note that the precise value of ϵ is not particularly important since the memory function for these networks maintains a value near 1 before falling sharply. This implies that an LRC network will be able to approximate any function $z(t) = \int_0^{T^*} d\tau h_1(\tau)u(t-\tau)$ for any kernel h_1 , so long as the network is large enough that its total linear memory obeys $\tau_\epsilon > T^*$.

MEMRISTOR RESERVOIRS

We now turn to establishing analogous results for memristor reservoirs. To begin, in the supplemental material we prove the following result:

Feasibility of Memristor Networks. *Reservoirs of networked memristors satisfy local fading memory and state separation properties for sufficiently weak input signal.*

Specifically, the proof requires that the driving signal satisfy $\|\vec{u}(t)\|_2 \leq \frac{(1-\chi)^2\alpha\beta}{\chi}$. This result was a surprise given the passive nature of the memristor model but simulations have demonstrated the importance of weak driving to the fading memory property. The dependence on χ illustrates the constraints put on the driving signal by the nonlinearity of the memristors. The condition above illustrates a tradeoff between nonlinearity and volatility, governed by the decay constant α in maintaining the fading memory property. We also note that nonvolatile memristors have demonstrated a form of fading memory [2, 24], though it is not clear what is at the root of this effect. Certainly, saturation effects at the boundary of the devices can also lead to fading memory for a strong signal and this will be in the opposite regime to the bound above. It is certainly possible that different memristors show fading memory over a wider range of driving signals and for varying reasons, but our investigations have made it clear that the linear model will only satisfy the local fading memory property when weakly driven. In the supplemental material we also show that, so long as the dissipative term is bounded below by a linear function of \vec{v} , a very similar bound will hold.

Further work has shown that when strongly driven, mem-

ristor networks can enter a transiently chaotic state in which trajectories will diverge in time [7], in apparent violation of the local fading memory property. However, after this transiently chaotic phase of the dynamics, the system will approach a steady state under constant driving. Presently it is not clear whether systems that display transient chaos can form useful reservoirs when the driving signal is time-varying, as chaotic dynamics may recur repeatedly. Our simulations have indicated that maintaining the fading memory property is important, so all memristor networks we employ are in the weakly driven regime.

The trajectory of a single memristor governed by eqn. (19) has the Volterra series expansion

$$\eta(t) = \frac{1}{\beta} \int_0^\infty d\tau_1 e^{-\alpha\tau_1} u(t - \tau_1) + \frac{\chi}{\beta^2} \int_0^\infty d\tau_1 \int_{\tau_1}^\infty d\tau_2 e^{-\alpha\tau_2} u(t - \tau_1) u(t - \tau_2) + O(\chi^2), \quad (22)$$

(see supplemental material), where we have neglected boundary effects and where higher order kernels of the input are suppressed by higher powers of χ . We immediately note that the kernel functions are exponentially decaying at a rate α . This is consistent with the fading memory property, as any perturbation in u will have an exponentially decreasing effect on η as time goes on. The expansion makes it clear that memristor trajectories depend on higher powers of the driving signal $u(t)$. In this sense, memristors may be considered as a source of nonlinearity in electronic reservoirs.

As a generalization of the linear approximation task, we consider the approximation of an arbitrary 2nd order filter which depends on the input signal for a time T^* into the past. Specifically, we wish to approximate a function of the input with the form,

$$z(t) = \int_0^{T^*} d\tau_1 F_1(\tau_1) u(t - \tau_1) + \int_0^{T^*} d\tau_1 \int_0^{T^*} d\tau_2 F_2(\tau_1, \tau_2) u(t - \tau_1) u(t - \tau_2). \quad (23)$$

Approximating this function with memristors requires isolating terms related to the second order contribution to the trajectory in eqn. (22). To do this, we note that a reservoir of two memristors $\eta_+(t)$ and $\eta_-(t)$, each driven by $u(t)$ and $-u(t)$ respectively, allows us to construct their sum (away from the boundaries and up to terms of order $O(\chi^2)$) as

$$\eta_+(t) + \eta_-(t) \approx \frac{2\chi}{\beta^2} \int_0^\infty d\tau_1 \int_{\tau_1}^\infty d\tau_2 e^{-\alpha\tau_2} u(t - \tau_1) u(t - \tau_2),$$

which cancels all odd terms in $u(t)$ in eqn. (22). Including memristors in pairs thus allows the training procedure to isolate these quadratic components and learn their weights so as to approximate eqn. (23).

The $e^{-\alpha\tau}$ dependence of terms in the Wiener/Volterra series only allows a dependence on u on timescales of order $\frac{1}{\alpha}$.

A lower value of α will integrate a longer window of the previous history into the current state, but will also obscure the value of the input signal at any single time. In reservoir computing, the parameters of the circuit are randomized to generate linearly independent trajectories, which allows the training to isolate different components of the input signal. In memristor networks, this may be accomplished by varying α and β (the timescales of decay/excitation for memristors), by varying the amplitude of the driving, or by introducing disorder into the structure of the circuit Ω_A . We employ what we view as the most practical option, which is varying the amplitude of the driving signal. In networks, memristors are driven with a proximal voltage generator that varies in amplitude from $+S$ to $-S$ in equally spaced increments, where S is a constant that may be tuned.

In fig. 6 we show the quadratic memory function $m_2(\tau_1, \tau_2) = C[u(t - \tau_1)u(t - \tau_2)]$ for reservoirs composed of LRC, single memristors, paired memristors and memristor networks as shown in figs. 3 and 4. As expected, while the LRC reservoir produces excellent linear reconstructions, it shows very poor ability to reconstruct quadratic functions. Among memristors while single memristors show clear nonlinearity, paired memristors are markedly better and memristor networks show only a limited advantage over separate paired memristor sub-circuits.

While memristor reservoirs give us the ability to calculate quadratic functions of the input with high accuracy for short times, the total quadratic memory $\tau_\epsilon^{(2)}$ does not scale extensively as the size of the reservoir is increased. This can be seen from the fact that the memristor network reservoir, which is 28 times bigger than the ‘‘paired memristors’’ reservoir, has a similar total quadratic memory. In the next section we consider hybrid reservoirs of memristor and LRC components, which do demonstrate extensive scaling.

Hybrid Deep Reservoirs

The properties of LRC and memristor reservoirs may be combined to achieve improved scaling of the nonlinear memory. The reservoir structure we will examine uses the trajectories of a ‘‘surface layer’’ reservoir $\vec{x}_s(t)$ where voltage generators are driven by the input, $\vec{s}_s = \vec{v}u(t)$, to drive another ‘‘deep layer’’ reservoir \vec{x}_d [13]. The deep layer voltage generators are driven by the surface layer trajectories as $\vec{s}_d = C\vec{x}_s$ where C is a matrix of coupling coefficients whose structure is discussed below. As LRC and memristor components are kept in separate layers, these deep reservoirs inherit the feasibility properties of their sub-components. The training procedure uses all trajectories $\vec{x} = [\vec{x}_s, \vec{x}_d]$ in the regression.

As seen in fig. 6, the ability of memristors to calculate quadratic functions of the input occurs only over very short delays. On the other hand, LRC networks show excellent linear memory approximations but cannot reconstruct nonlinear functions. This would suggest that using a surface layer memristor network to generate nonlinear transformations of the input, and then using these to drive a deep layer LRC reservoir that would remember them, would give both good

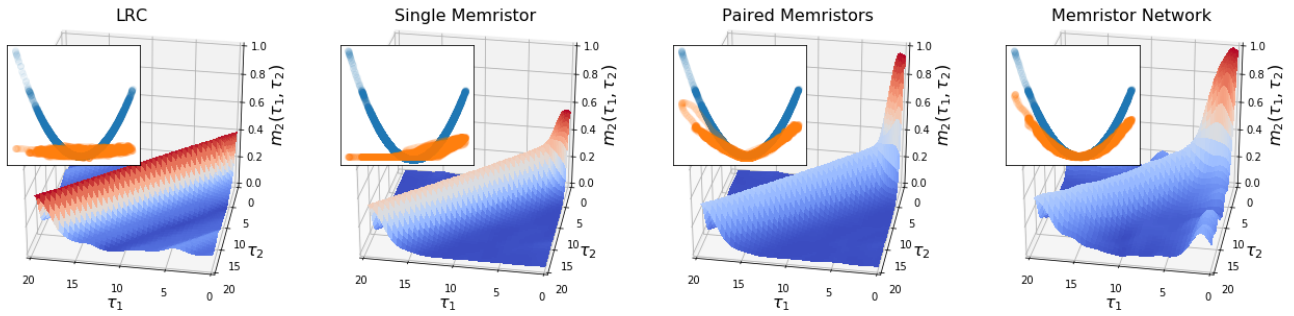


Figure 6. The quadratic memory function $m_2(\tau_1, \tau_2)$ for a single LRC sub-circuit (left), a single memristor sub-circuit (middle left), paired memristors sub-circuit (middle right) and a triangular lattice of memristors (right) as shown in figs. 3 and 4. This measures the reservoir's ability to approximate the function $z(t) = u(t - \tau_1)u(t - \tau_2)$. The colors of the surfaces are purely for visualization and values should be read from the z-axis which all extend from 0 to 1. We define $\tau^* := \operatorname{argmax}_{\tau} m_2(\tau, \tau)$, the optimal delay for an equal-time reconstruction; the insets show the corresponding reconstruction \hat{z} (orange) and target output $z(t) = [u(t - \tau^*)]^2$ (blue) as a function of the input signal $u(t - \tau^*)$. As expected, the LRC circuit is only capable of generating linear approximations of the output. A single memristor reservoir is unable to isolate its quadratic component and misses negative parts of the reconstruction due to boundary effects (middle left inset). The addition of another memristor with opposite bias, significantly increases the ability to reconstruct z . The memristor network shows an enhanced ability to reconstruct z and clear nonlinearity (right inset). The nonlinear memory function value of $m_2(\tau^*, \tau^*)$ for each network was 0.390 (LRC), 0.558 (single memristor), 0.960 (paired memristors), and 0.995 (memristor network).

quadratic reconstructions and long memory of these reconstructions. In fig. 8, the top panel shows the result of using a pair of memristors configured as in the section above, to drive an LRC reservoir. Each of the two memristor trajectories in $\vec{x}_s = [\eta_+(t), \eta_-(t)]$ is used as a source signal for a small LRC reservoir of 10 circuits, which we index by $n \pm$ with $n = 1 \dots 10$. Each LRC circuit produces 2 trajectories $q_{n\pm}, \dot{q}_{n\pm}$ giving a total of $2 + 2 \times 10 \times 2 = 42$ output trajectories. The LRC trajectories are calculated by eqn. (14) with $s_{n\pm} = \eta_{\pm}$. The index n determines the parameters of the LRC elements given $\gamma = 0.4$ and $\Delta\omega = 0.4$ and eqn. (21).

The resulting reservoir trajectories are used to evaluate the quadratic memory function in the top panel of fig. 8 with the

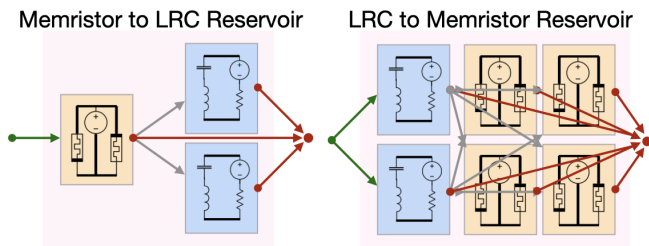


Figure 7. We consider two deep reservoir structures in which the layers are independent sub-circuit reservoirs of LRC or memristor sub-circuits. Connections and layers are shown schematically to make the figures legible. Inputs to the reservoirs are shown in green, internal connections between layers are shown in grey and outputs are shown in red. In the memristor to LRC reservoirs (left), the surface layer is a paired memristor circuit. Each of the output trajectories $\eta_{\pm}(t)$ is used to drive a deep layer reservoir of 10 LRC sub-circuits. In the LRC to memristor reservoirs (right) each pair of surface layer LRC circuits drives 12 paired memristor circuits (not all shown here) such that all sums and differences of the 4 LRC trajectories drive a separate paired memristor circuit.

results showing a substantial increase in the reservoir's computational capacity for 'equal-time' quadratic reconstructions (defined via $m_2(\tau, \tau)$). As the deep LRC reservoir is used to recall the equal-time products computed by the memristor reservoir, we expect that measures of their total quadratic memory $\tau_{\epsilon}^{(2)}$ will also scale extensively. However increasing the reservoir size will not improve the reconstruction of unequal-time products where $\tau_1 \neq \tau_2$.

We next consider using a surface layer LRC reservoir to drive a deep layer memristor reservoir. As guiding intuition, if we consider the LRC reservoir as computing the Fourier transform of the signal, the deep memristor layer will calculate products of this transform, akin to a 2-dimensional Fourier transform in τ_1 and τ_2 . We predict that the resulting network will display an improved unequal-time quadratic memory function. To test this, we implemented the same 10 circuit LRC reservoir as described above driven with the same input signal u . The resulting 20 trajectories, $q_n, \dot{q}_n, n = 1 \dots 10$ are used to drive a set of memristor pairs such that the sum and difference of every pair of the 20 LRC trajectories are used to drive an independent pair of memristors. This means that for a particular pair η_{m+}, η_{m-} , the driving signal may be $q_n \pm q_{n'}, q_n \pm \dot{q}_{n'}$ or $\dot{q}_n \pm \dot{q}_{n'}$ such that all pairs n, n' and q, \dot{q} are used. The resulting $2 \times 20 \times 19 + 20 = 780$ trajectories are used to train the reservoir. In the lower panel of fig. 8, we calculate the quadratic memory function for this architecture. We observe a substantial improvement in the reservoir's ability to construct unequal-time products of the input signal. Although this requires a significant increase in the size of the reservoir, such an increase is expected. The number of unequal-time products with $\tau_1, \tau_2 < T^*$ scales quadratically in the maximum delay T^* and so the reservoir size must scale similarly.

In fig. 9 we show the scaling of the total quadratic memory $\tau_{0,1}^{(2)}$ with the size of the reservoir. The total quadratic memory

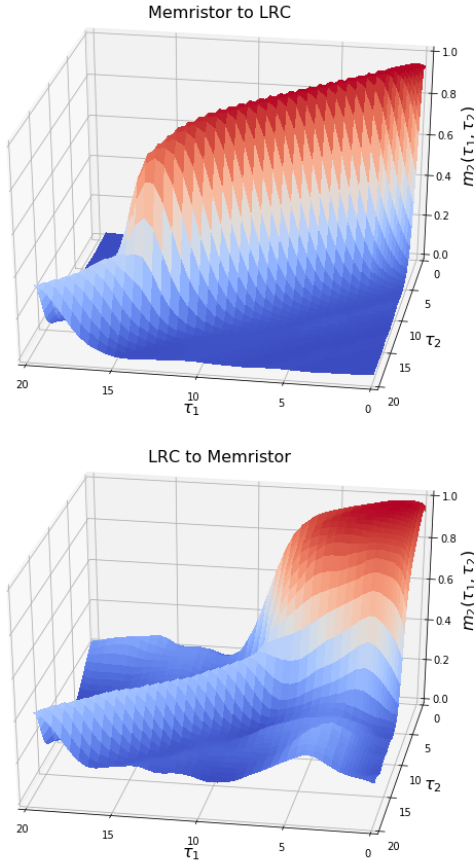


Figure 8. The quadratic memory function $m_2(\tau_1, \tau_2)$ for the hybrid memristor and LRC reservoirs shown in fig. 7. The top panel shows the result of using a driven pair of memristors to drive an LRC reservoir. The LRC reservoir stores memory of the nonlinear computation in the memristor network, leading to large equal-time quadratic capacities. In the lower panel, the result of using an LRC reservoir to drive a set of memristor pairs is shown. The memristor pairs compute products of the trajectories generated in the LRC network, approximately implementing a 2-dimensional Fourier transform. This extends the quadratic memory function to longer delays compared with the paired memristor reservoir in fig. 6. The LRC circuits were arranged with $\gamma = 0.4$, $\Delta\omega = 0.4$ corresponding to a cutoff frequency of $4 Hz$

indeed scales extensively with the size of the reservoir indicating that arbitrary unequal-time products may be reconstructed by a sufficiently large reservoir. Estimating these quantities accurately turns out to be quite subtle, as estimated values will display strong bias when calculated on a finite interval. In the supplemental material we show how finite size scaling can be used to obtain reliable estimates. We emphasize that it is the total nonlinear memory $\tau_e^{(2)}$ that can scale extensively with the system size; increasing the maximum delay T^* under which we can reconstruct products of the input will require that the reservoir size scale as T^{*2} .

Another natural architecture to consider would use memristor reservoirs as both surface and deep layers, as has been

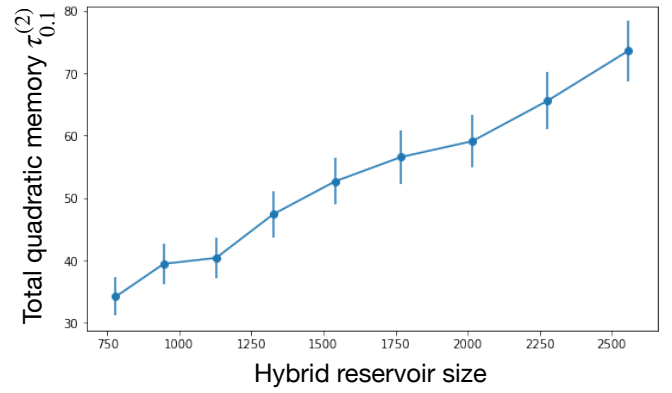


Figure 9. The scaling of the total quadratic memory with reservoir size in the hybrid LRC to Memristor reservoir. LRC reservoirs ranging from 10 to 18 sub-circuits were used to drive a memristor reservoir as described in the main text, resulting in reservoirs ranging from 946 to 2556 internal degrees of freedom. The total quadratic memory $\tau_{0.1}^{(2)}$ (and errorbars) were estimated from a finite size scaling analysis as detailed in the supplemental material.

considered in works based on the simulation of these devices. Given the discussion above, we expect the primary benefit of this architecture would be to enhance higher order nonlinear capacities, which is precisely what we observe in simulation. However, as this is outside the scope of the computational task we set out to achieve, we do not include results from such networks here.

Comparison with Echo State Networks

To show that these design considerations lead to improved performance, we construct a fitting task in which we must approximate a known function of the input signal. We construct the following target output:

$$z(t) = \int_0^{10} d\tau K_1(\tau_1)u(t - \tau_1) + \int_0^{10} d\tau_1 \int_0^{10} d\tau_2 K_2(\tau_1, \tau_2)u(t - \tau_1)u(t - \tau_2) \quad (24)$$

where the kernels K_1 and K_2 are defined as

$$K_1(\tau_1) = e^{-0.5\tau_1} \cos(2\tau_1) \quad (25)$$

$$K_2(\tau_1, \tau_2) = -e^{-0.3(\tau_1 + \tau_2)} \cos(2(\tau_1 - \tau_2)). \quad (26)$$

Accurate approximation of this output requires a mixture of memory and nonlinearity.

In addition to the hybrid reservoir discussed above, we also apply an implementation of continuous time Echo State Networks (ESNs)[16, 20] for comparison. An ESN is a dynamical reservoir in which the internal states evolve according to

$$\dot{\vec{x}} = -\alpha\vec{x}(t) + \tanh(M\vec{x}(t) + \vec{v}u(t)), \quad (27)$$

where α is a decay term, $\tanh(\cdot)$ applies to every neuron, M is a matrix that in order to satisfy the fading property must have

Table I. Comparison of reservoir performance on the quadratic filtering task described in the main text.

Reservoir	$\dim(\vec{x})$	nMSE	Gen. nMSE
Pure Memristor Network	800	0.1	2.
ESN	780	0.02	0.03
LRC→Memristor	780	0.01	0.01

maximum eigenvalue less than one, and \vec{v} scales the magnitude of the input $u(t)$ which drives each neuron.

We compare the results of a suitably tuned ESN to a pure memristor network as in fig. 4, and a hybrid surface LRC to deep memristor reservoir. The memristor network is a 17×17 triangular lattice with 800 edges each containing a memristor ($\alpha = 3$, $\beta = 1$, $\chi = 0.8$) and voltage generator. The elements of \vec{v} were uniformly distributed on the interval $[-1, -0.1] \cup [0.1, 1]$. The LRC→Memristor reservoir was configured identically to that presented in the previous section and included a total of 780 trajectories. Finally the ESN consisting of 780 elements was run and tuned following the recommendations in [20]. As far as possible, each reservoir was configured to produce the same number of trajectories (the lattice structure of the naive memristor network imposes some constraints). Further details on the implementation of each reservoir can be found in the supplemental material. The LRC→Memristor reservoir was configured identically to that presented in the previous section and included a total of 780 trajectories. Finally the ESN consisting of 780 elements was run and tuned following the recommendations in [20].

Each reservoir was first initialized on the interval $[0, 100]$ corresponding to approximately 100 autocorrelation times of the input driving signal. They were then trained on the interval $[100, 4000]$ and the $\text{nMSE}_{[100,4000]}$ is reported in table I. Lastly, a generalization error is reported by calculating the $\text{nMSE}[z]$ on the interval $[4000, 5000]$ with the weights that were trained on $[100, 4000]$. The generalization error is no longer normalized to $[0, 1]$ as the weights are calculated on a different interval. However it is the most important measure of the reservoir’s ability to approximate the function $u \mapsto z$, rather than to simply fit this function on a single training interval.

The results of the training are shown in table I. The hybrid LRC→Memristor reservoir demonstrates a 10-fold improvement over the pure memristor network and performs on par with the ESN implementation in training as well as a 2-fold improvement in generalization error. We attribute this to the specialized structure of the LRC to memristor reservoir, which gives it an advantage at reliably calculating quadratic functions of the input. We conclude that suitably crafted analog reservoirs are thus capable of matching and even surpassing the performance of standard reservoirs. The generalization error of the pure memristor network exceeded 1, and shows that the MSE on this interval was twice the variation in z . This indicates no ability to generalize the fit from the training interval and highlights the importance of reporting generalization error, rather than training error, in work on electronic reservoirs.

DISCUSSION

Despite wide interest in utilizing electronic circuits with memory for hardware reservoirs, an understanding of how these systems process and store information has been lacking. For echo state networks, the balance between memory and nonlinearity is controlled primarily by the spectral radius of the coupling matrix. However, no similar conditions have been explored for electronic networks.

In this work we have shown that linear electronic reservoirs of LRC circuits can be constructed with optimal memory properties, having an eigenvalue spectrum known to correspond to an extensive memory (e.g. that scales proportionally to the number of components). This may be interpreted as performing a Fourier transform of the driving signal in hardware, where the eigenvalue spectrum required can be designed appropriately for a given problem.

In memristor reservoirs, we have shown that while the system contains contributions from terms of very high order, these are moderated in strength by powers of χ . It is essential that the reservoir be able to isolate desired terms to make use of them in the training process. We have shown that using paired memristors of opposite polarity gives a substantial increase in the reservoir’s ability to isolate their quadratic kernels.

Combining LRC and memristor networks into deep reservoirs allows the utilization of the memory capabilities of LRC reservoirs and the nonlinear capacities of memristor reservoirs in order to achieve specific computational goals. Utilizing an LRC network as a deep layer allows nonlinear computations performed in the surface memristor network to be stored for long times. Similarly, using an LRC reservoir as the surface layer to drive a deep layer memristor network will calculate products of Fourier modes and give enhanced unequal-time quadratic capacities. Most importantly, this leads to a total quadratic memory which scales extensively in the system size, such that arbitrary products of the input can be constructed by a sufficiently large reservoir.

This analysis can have substantial impacts on performance, as we show in our comparison to ESN reservoirs. The hybrid reservoirs we present give a 10-fold improvement over the naive memristor network implementation, and perform on par with the ESN implementation. Properly constructed electronic reservoirs should thus be capable of matching the performance of standard reservoirs but also allow the use of larger reservoirs and faster computation times.

Our approach to the analysis of the computational capacities of memristor and LRC reservoirs can be generalized to higher order kernels of the network and to other nonlinear elements. In this sense we present a general approach to the understanding of physical reservoirs, in analogy to the methods available to tune ESNs by trading between memory storage and nonlinearity [20].

ACKNOWLEDGEMENTS

The work of FC and FCS was carried out under the auspices of the NNSA of the U.S. DoE at LANL under Contract

No. DE-AC52-06NA25396. FC was also financed via DOE-ER grant PRD20190195, and FCS by a CNLS Fellowship and 20190195ER. Revision of this manuscript by FCS was performed while employed at the London Institute for Mathematical Sciences. AK was supported by grant number FQXi-

RFP-IPW-1912 from the Foundational Questions Institute and Fetzer Franklin Fund, a donor advised fund of Silicon Valley Community Foundation. AK thanks the Santa Fe Institute for helping to support this research.

-
- [1] Appeltant, L., Soriano, M. C., Van der Sande, G., Danckaert, J., Massar, S., Dambre, J., Schrauwen, B., Mirasso, C. R., and Fischer, I. (2011). Information processing using a single dynamical node as complex system. *Nature communications*, 2(1):1–6.
- [2] Ascoli, A., Tetzlaff, R., Chua, L. O., Strachan, J. P., and Williams, R. S. (2016). History erase effect in a non-volatile memristor. *IEEE Transactions on Circuits and Systems I: Regular Papers*, 63(3):389–400.
- [3] Athanasiou, V. and Konkoli, Z. (2020). On improving the computing capacity of dynamical systems. *Sci. Rep.*, 10(9191).
- [4] Bertschinger, N. and Natschläger, T. (2004). Real-time computation at the edge of chaos in recurrent neural networks. *Neural computation*, 16(7):1413–1436.
- [5] Boyd, S. and Chua, L. (1985). Fading memory and the problem of approximating nonlinear operators with volterra series. *IEEE Transactions on circuits and systems*, 32(11):1150–1161.
- [6] Caravelli, F. and Carbajal, J. P. (2018). Memristors for the curious outsiders. *Technologies*, 6(4):118.
- [7] Caravelli, F., Sheldon, F. C., and Traversa, F. L. (2021). Global minimization via classical tunneling assisted by collective force field formation.
- [8] Caravelli, F., Traversa, F. L., and Di Ventra, M. (2017). Complex dynamics of memristive circuits: Analytical results and universal slow relaxation. *Physical Review E*, 95(2):022140.
- [9] Carbajal, J. P., Dambre, J., Hermans, M., and Schrauwen, B. (2015). Memristor models for machine learning. *Neural Computation*, 27(3).
- [10] Chua, L. (1971). Memristor—the missing circuit element. *IEEE Transactions on circuit theory*, 18(5):507–519.
- [11] Dambre, J., Verstraeten, D., Schrauwen, B., and Massar, S. (2012). Information processing capacity of dynamical systems. *Scientific reports*, 2:514.
- [12] Du, C., Cai, F., Zidan, M. A., Ma, W., Lee, S. H., and Lu, W. D. (2017). Reservoir computing using dynamic memristors for temporal information processing. *Nature communications*, 8(1):2204.
- [13] Gallicchio, C., Micheli, A., and Pedrelli, L. (2017). Deep reservoir computing: A critical experimental analysis. *Neurocomputing*, 268(13):87–99.
- [14] Hermans, M. and Schrauwen, B. (2010). Memory in linear recurrent neural networks in continuous time. *Neural Networks*, 23(3):341–355.
- [15] Inubushi, M. and Yoshimura, K. (2017). Reservoir computing beyond memory-nonlinearity trade-off. *Scientific reports*, 7(1):10199.
- [16] Jaeger, H. (2001). The “echo state” approach to analysing and training recurrent neural networks—with an erratum note. Technical Report 148.34, Bonn, Germany: German National Research Center for Information Technology GMD.
- [17] Jaeger, H. (2002). Short term memory in echo state networks. gmd-report 152. In *GMD-German National Research Institute for Computer Science (2002)*, <http://www.faculty.jacobs-university.de/hjaeger/pubs/STMEchoStatesTechRep.pdf>. Cite-seer.
- [18] Jaeger, H. and Haas, H. (2004). Harnessing nonlinearity: Predicting chaotic systems and saving energy in wireless communication. *Science*, 304(5667):78–80.
- [19] Kulkarni, M. S. and Teuscher, C. (2012). Memristor-based reservoir computing. In *2012 IEEE/ACM International Symposium on Nanoscale Architectures (NANOARCH)*, pages 226–232. IEEE.
- [20] Lukoševičius, M. (2012). A practical guide to applying echo state networks. In *Neural networks: Tricks of the trade*, pages 659–686. Springer.
- [21] Maass, W., Joshi, P., and Sontag, E. D. (2007). Computational aspects of feedback in neural circuits. *PLoS Comput Biol*, 3(1):e165.
- [22] Maass, W., Natschläger, T., and Markram, H. (2002). Real-time computing without stable states: A new framework for neural computation based on perturbations. *Neural computation*, 14(11):2531–2560.
- [23] Marinella, M. J. and Agarwal, S. (2019). Efficient reservoir computing with memristors. *Nature Electronics*, 2:1–2.
- [24] Menzel, S., Waser, R., Siemon, A., La Torre, C., Schulten, M., Ascoli, A., and Tetzlaff, R. (2017). On the origin of the fading memory effect in rerams. In *2017 27th International Symposium on Power and Timing Modeling, Optimization and Simulation (PATMOS)*, pages 1–5. IEEE.
- [25] Moon, J., Ma, W., Shin, J. H., Cai, F., Du, C., Lee, S. H., and Lu, W. D. (2019). Temporal data classification and forecasting using a memristor-based reservoir computing system. *Nature Electronics*, 2(10):480–487.
- [26] Pathak, J., Hunt, B., Girvan, M., Lu, Z., and Ott, E. (2018). Model-free prediction of large spatiotemporally chaotic systems from data: A reservoir computing approach. *Physical review letters*, 120(2):024102.
- [27] Strukov, D. B., Snider, G. S., Stewart, D. R., and Williams, R. S. (2008). The missing memristor found. *Nature*, 453(7191):80–83.
- [28] Tanaka, G., Yamane, T., Héroux, J. B., Nakane, R., Kanazawa, N., Takeda, S., Numata, H., Nakano, D., and Hirose, A. (2019). Recent advances in physical reservoir computing: A review. *Neural Networks*, 115:100–123.
- [29] Torrejon, J., Riou, M., Araujo, F. A., Tsunegi, S., Khalsa, G., Querlioz, D., Bortolotti, P., Cros, V., Yakushiji, K., Fukushima, A., et al. (2017). Neuromorphic computing with nanoscale spintronic oscillators. *Nature*, 547(7664):428–431.
- [30] Wang, R., Yang, J.-Q., Mao, J.-Y., Wang, Z.-P., Wu, S., Zhou, M., Chen, T., Zhou, Y., and Han, S.-T. (2020). Recent advances of volatile memristors: Devices, mechanisms, and applications. *Advanced Intelligent Systems*, 2(9):2000055.
- [31] White, O. L., Lee, D. D., and Sompolinsky, H. (2004). Short-term memory in orthogonal neural networks. *Physical review letters*, 92(14):148102.
- [32] Zegarac, A. and Caravelli, F. (2019). Memristive networks: From graph theory to statistical physics. *EPL (Europhysics Letters)*, 125(1):10001.

Supplemental Materials: The Computational Capacity of LRC, Memristive and Hybrid Reservoirs

Forrest C. Sheldon* and Francesco Caravelli
*Theoretical Division and Center for Nonlinear Studies,
Los Alamos National Laboratory, Los Alamos, New Mexico 87545, USA*

Artemy Kolchinsky
Santa Fe Institute, 1399 Hyde Park Road, Santa Fe, NM 87501, USA

CONTENTS

I. The Computational Capacity of Continuous Time Reservoirs	1
1. Measures of Capacity	2
II. Input Signal	3
III. Reservoir Training	3
A. Solution of the Minimum Squared Error	3
B. Training Procedure	3
IV. Figure Details	4
A. LRC simulations	4
B. Quadratic Capacity Figure	5
C. Hybrid Network Figure	6
D. Linear and Quadratic Memory Scaling	6
E. Comparison to Echo State Networks	6
V. Proof of computational capacity bound	7
VI. Feasibility Properties of LRC reservoirs	8
A. Fading Memory	10
B. State Separation	10
VII. Feasibility Properties of Memristor Reservoirs	10
A. Fading Memory	11
B. State Separation	11
VIII. Solution of LRC circuits	12
IX. Volterra Series Solution of Memristor Equations	13
X. Finite Size Scaling of Quadratic Memory Capacities	14
References	14

I. THE COMPUTATIONAL CAPACITY OF CONTINUOUS TIME RESERVOIRS

A framework for defining and assessing the computational capacity of reservoirs was developed by Dambre *et al.* [2] in the context of discrete time reservoirs. Here we deal with its extension to continuous time reservoirs [3].

* To whom correspondence should be addressed. E-mail: fs@lms.ac.uk; Current Address: London Institute for Mathematical Sciences, 21 Albemarle St. London, W1S 4BS, UK

The goal of reservoir computing is to approximate the function $z : u \mapsto z[u]$, rather than simply the value of this function $z(t)$ on the training interval $t \in [0, T]$. By this we mean that after training, the learned weights should still accurately approximate $z[u]$ outside of the training interval. To formalize this notion, Dambre introduces a ‘‘fading memory Hilbert space’’ consisting of functions which possess the fading memory property (i.e., they depend only on the recent history of the input). The reservoir trajectories $\vec{x}[u](t)$ and output trajectory $z[u](t)$ are members of this space by assumption.

Defining this Hilbert space revolves around the construction of an inner product. As members of the space are functions that take an input u , the inner product must depend on the space of inputs u . The inner product on the space of trajectories is constructed by first requiring that a measure over inputs u is specified, and then defining the inner product between two elements of the Hilbert space z, z' as $\langle z, z' \rangle_u = E_u [\int_0^\infty z[u](t) z'[u](t) dt]$, where E_u indicates expectation over the measure.

Of course, an inner product defined this way would be very difficult to compute. Instead we appeal to ergodicity: For well behaved functions of u (finite variance and with covariance tending to zero for long times) the time average will converge to the average calculated over the measure. For the case of the inner product above, it means that we can ‘‘measure’’ these quantities from simulations by simulating the reservoir for a sufficiently long time. As an example, when driven for a sufficiently long time, the time average ($\frac{1}{T} \int dt \cdot = \langle \cdot \rangle_T$) of the product of two reservoir trajectories $x_1[u](t)$ and $x_2[u](t)$ should converge to their inner product on the Hilbert space,

$$\lim_{T \rightarrow \infty} \langle x_1(t), x_2(t) \rangle_T - \langle x_i[u], x_j[u] \rangle_u = 0. \quad (1)$$

Interested readers should consult [2], esp. the supplementary material. Estimating these values from simulations can be strongly subject to bias in the convergence. For this reason we employ a finite size scaling analysis to extract long-time values from their finite time simulation estimates.

The notion of distance induced by the inner product is estimated by the MSE given in the text

$$\text{MSE}[z_1, z_2]_T \rightarrow \langle (z_1(t) - z_2(t))^2 \rangle_u. \quad (2)$$

We will not make heavy use of this Hilbert space, keeping reference to time averages in calculating MSE. However, we note that these may be regarded as finite time estimates of the quantities of interest which are defined over the Hilbert space. In subsequent sections, we use a finite size scaling analysis to extract estimates of these quantities as $T \rightarrow \infty$. Importantly, by averaging over sufficiently long times we can regard our results as measuring properties of the *reservoir* rather than the particular time interval used for training. We also inherit the linear structure of the Hilbert space with notions of orthogonality, dimension and distance.

1. Measures of Capacity

We are interested in the estimator that minimizes the MSE for some target output z . Following Dambre *et al.* [2], we define the capacity of the dynamical system to approximate z as

$$C_T[z] = 1 - \frac{\min_{\vec{w}} \text{MSE}_T[z, \vec{w}^T \vec{x}]}{\langle z^2 \rangle_T}, \quad (3)$$

where $\langle f \rangle_T = \frac{1}{T} \int_0^T dt f(t)$. The capacity is bounded $0 \leq C_T[z] \leq 1$. In what follows, in addition to the capacity $C_T[z]$, we will also reference the normalized mean-squared error of the estimate, $\text{nMSE}_T[z] = 1 - C_T[z]$.

The capacity above is an estimate of the inner product on the Hilbert space. An immediate consequence is that, when capacities are evaluated on a complete set of orthogonal functions and in the long time limit, their sum will tend towards the number of linearly independent trajectories in the reservoir, i.e., the dimension of the span of the reservoir trajectories. As shown in [2], this results in a tradeoff between the total linear memory of a reservoir, and its total nonlinear memory[4].

By evaluating $C_T[z]$ for different choices of z , one can quantify the capacity of the reservoir to perform different kinds of computations. For example, when z is a linear function of the input u , $C_T[z]$ will quantify capacity to perform linear computations, and when z is a nonlinear function of the input u , $C_T[z]$ will quantify capacity to perform nonlinear computations. Given this, we note two points that will guide our development of electronic reservoirs: (1) Since an approximation can only be accurate when $z[u]$ is close to the span of the the reservoir trajectories, a reservoir must be tunable, by which we mean that it can be designed so as to achieve high $C_T[z]$ for different desired choices of z . For echo state networks, various rules of thumb for tuning their performance have been developed; we present analogous methods for obtaining high values of specific $C_T[z]$ in electronic networks; (2) Based on these capacities, we can build a measure of total memory (see τ_ϵ below) which should scale with the size of the reservoir. The success of RC draws from the ability to use very large reservoirs. If electronic reservoirs are to be useful, increasing the size of the reservoir must improve its performance on the type of capacities we chose in (1). Optimal scaling is extensive in the system size. In the main text we develop measures of capacity for different families of functions z that we will be interested in.

II. INPUT SIGNAL

The notions of computational capacity were originally developed in the context of discrete time reservoirs. Central to the introduction of the fading memory Hilbert space is the definition of an inner product between functions in terms of an expectation over an ensemble of input signals. Specifically, for functions $z[u]$ and $z'[u]$ that depend only on the previous h timesteps, the inner product between these is defined as the expectation over the ensemble of previous histories, $\langle z, z' \rangle = E_{U^h}[zz']$ where U^h is the space of previous histories where each timestep is i.i.d. sampled from a distribution $p(u)$. The resulting input signals are uncorrelated $\langle u(t - \tau_1)u(t - \tau_2) \rangle = \sigma^2 \delta_{\tau_1, \tau_2}$. The computational capacity for reconstructing linear functions of the input thus measure the ability to recall the exact state of the input signal at some previous time.

In continuous time we must cope with the introduction of the timescale of our reservoir. A dynamical system will have some characteristic timescale over which it can vary and will generally display an autocorrelation function that is decreasing with the time difference on that same timescale, *e.g.* for a system with timescale t^* , $\langle \eta(t)x(t - \tau) \rangle = f(\tau/t^*)$. In formulating an input signal we have two options for how to proceed.

One would be to drive the system with a noise process $\xi(t)$ which maintains the uncorrelated feature of the driving process from discrete time, $\langle \xi(t)\xi(t - \tau) \rangle = 2D\delta(\tau)$. The reservoir would no longer be able to construct the rapid variations of the noise process, but we could assess how well the system computed various filters of this noise, for example $z(t) = \int_0^\infty d\tau e^{-\alpha\tau} \xi(t - \tau)$. In this setting however, the connection to previous work is indirect and requires choosing particular timescales in which to perform memory reconstructions.

Alternatively, following [3] we can produce a signal that varies on the appropriate timescale by filtering a noise process and utilize this as the driving signal of our reservoir. We choose to proceed along this route as it most resembles the tasks towards which reservoir computing is applied. As a signal, we elected to use gaussian white noise smoothed by a double-exponential window with a timescale $1/a$

$$u(t) = \int_{-\infty}^{\infty} d\tau e^{-a|t-\tau|} \xi(\tau) \quad (4)$$

where

$$\langle \xi(t) \rangle = 0, \quad \langle \xi(t)\xi(t') \rangle = D\delta(t - t'). \quad (5)$$

Applying these relationships we have $\langle u(t) \rangle = 0$ and $\langle u(t)u(t + \tau) \rangle = D(\tau + \frac{1}{a})e^{-a\tau}$. We thus obtain random input signal with unit autocorrelation time and unit variance by choosing $D = 1$, $a = 1$. Note that over short times the characteristic timescale is $\frac{1}{2a}$.

In figure 1 we show a sample input signal trajectory (top panel), the resulting autocorrelation function (middle panel) and the resulting power spectral density (bottom panel). The autocorrelation function panel contains both a sample autocorrelation function, calculated from a single trajectory of the input, and the analytical autocorrelation function above.

III. RESERVOIR TRAINING

A. Solution of the Minimum Squared Error

For an input u , output z and reservoir trajectories \vec{x} , the reservoir output weights are chosen as the minimizer of the mean square error. Defining the time average, $\langle f \rangle_T = \frac{1}{T} \int_0^T dt f(t)$, we can write this as

$$\text{MSE}_T[z, \vec{w}^T \vec{x}'] = \langle (z - \vec{w}^T \vec{x}')^2 \rangle_T. \quad (6)$$

As this objective is convex and differentiable we can find the optimum by taking the derivative,

$$\frac{\partial}{\partial w_i} \text{MSE}_T[z, \vec{w}^T \vec{x}'] = 2\langle x_i z \rangle_T - 2\hat{w}^T \langle \vec{x}' x_i \rangle_T = 0 \quad (7)$$

The solution to the resulting system of equations is $\hat{w} = \langle \vec{x}' \vec{x}'^T \rangle_T^{-1} \langle \vec{x}' z \rangle_T$.

B. Training Procedure

Once a set of trajectories $\vec{x}(t)$ were generated on the interval $[0, 5000]$ the portion of the trajectory on $[0, 100]$ was removed as a transient. The remaining trajectories had a constant vector appended and training was then performed using scikit-learn's Ridge regression method. In all cases the ridge regression parameter was set to $k = 0.0001$ such that the regularization of the weights was minimal.

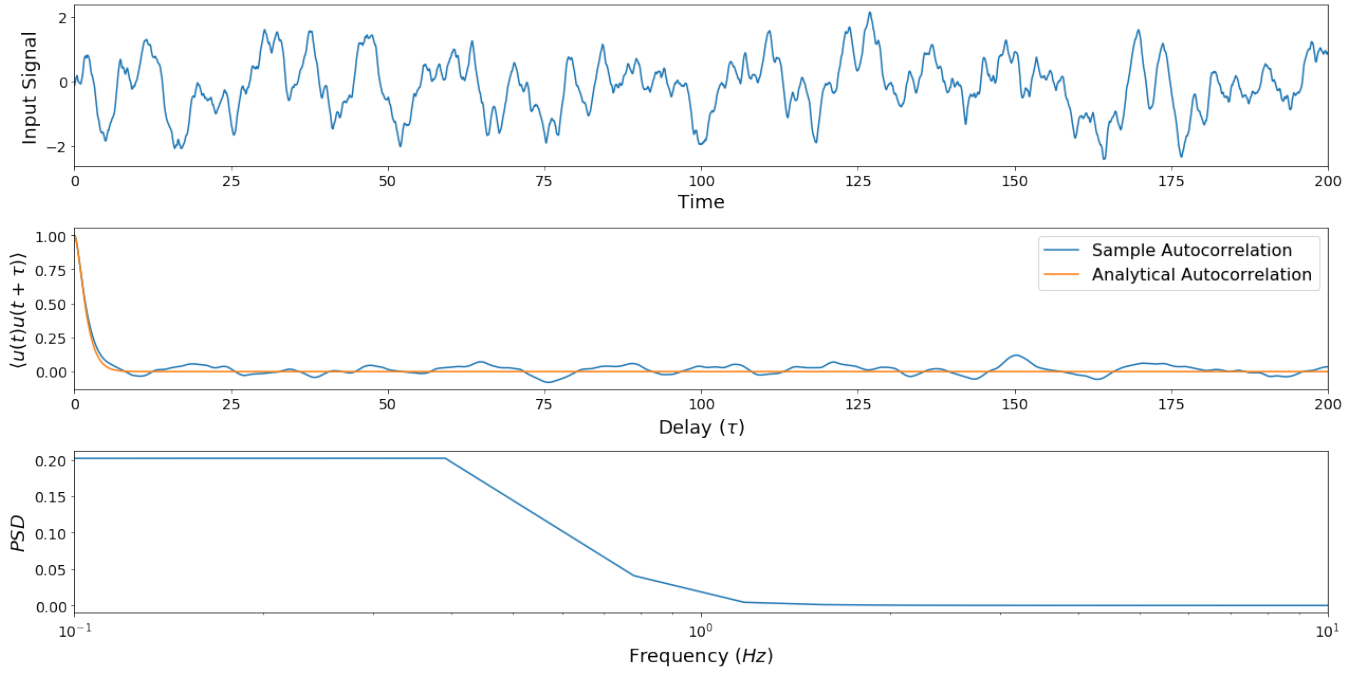


Figure 1. A sample input signal trajectory (top panel), corresponding autocorrelation function (middle panel) and power spectral density (PSD) (bottom panel). The input signal was constructed by smoothing Gaussian white noise with a double exponential window with time constant $1/a$. The resulting autocorrelation function displays a long time exponential decrease as $e^{-a\tau}$. In simulations we set $a = 1$. The power spectral density of the resulting signal contains significant contributions only from frequencies below 1.

IV. FIGURE DETAILS

A. LRC simulations

The memory function was calculated by following the training prescription above for various signal delays τ . For the scaling figure, LRC reservoirs of sizes $N = 10, \dots, 18$ were simulated with $\delta\omega = \gamma = 4/N$. Once simulated, a bijective search was performed to find the smallest τ at which the memory function satisfied $m(\tau) < 1 - \epsilon$. The tolerance on the search was set to 1 which also determined the errorbars. A finite size scaling analysis was performed but is unnecessary as the memory capacities quickly converge to their asymptotic values. In this case, we can in fact observe by directly constructing the kernel of the reservoir.

For a linear network, the kernel of the reservoir can be reconstructed from the fitted weights. Specifically, we can write the predicted output as

$$\hat{z}(t) = \sum_{n=1}^N (w_{q_n} q_n(t) + w_{\dot{q}_n} \dot{q}_n(t)) + w_c \quad (8)$$

$$= \int_0^\infty d\tau K(\tau) u(t - \tau) + w_c. \quad (9)$$

where K indicates the kernel function,

$$K(\tau) = e^{-\gamma\tau} \sum_{n=1}^N \frac{1}{l_n n \Delta\omega} \left[w_{q_n} \sin(n\Delta\omega\tau) + w_{\dot{q}_n} (n\Delta\omega \cos(n\Delta\omega\tau) - \gamma \sin(n\Delta\omega\tau)) \right], \quad (10)$$

which gives an explicit representation of the network's approximation to $\delta(t - \tau)$. The functions q_n, \dot{q}_n are drawn from the reservoir solution in 11. In Figure 2, we display the memory function, kernel and reconstruction for an LRC circuit reservoir with $\gamma = 0.12$, $\Delta\omega = 0.7\gamma$ and 71 subcircuits (motifs) corresponding to an cutoff frequency of $N\Delta\omega = 6Hz$. We can see that the memory function can reconstruct the signal with a fairly long delay. Achieving an estimate of the exact representation of the kernel in eqn. (10) required a close correspondence between simulations and the exact formula over many autocorrelation times of a rapidly oscillating system. As most integration schemes would lead to a small buildup of phase differences over these

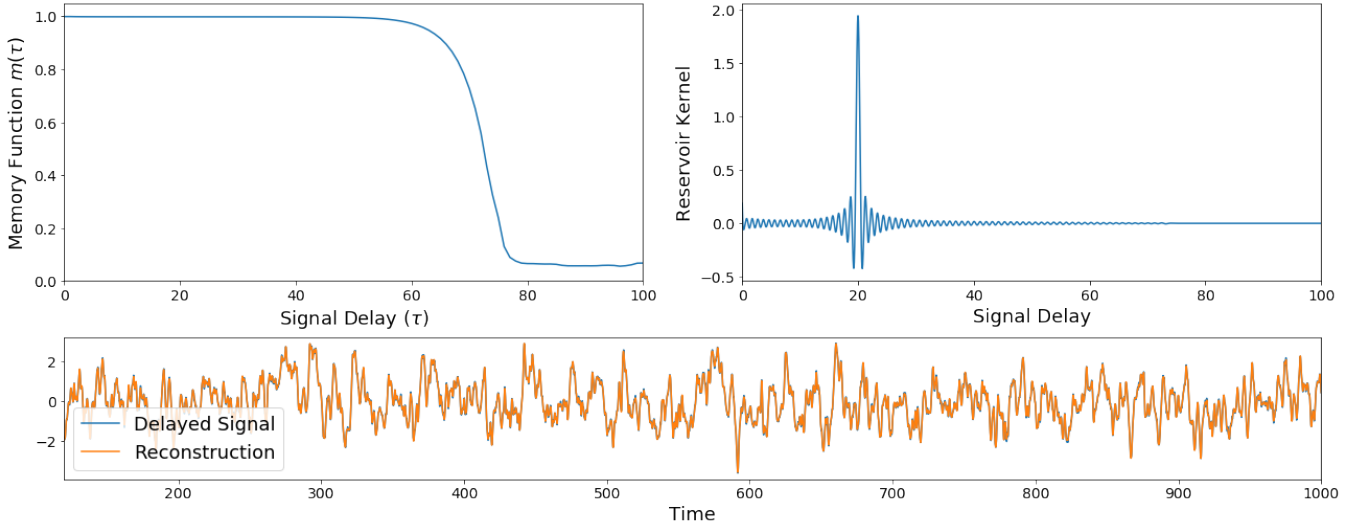


Figure 2. The (linear) memory function $m(\tau)$ (upper left), kernel (upper right) and reconstruction (lower) for an LRC circuit reservoir with $\gamma = 0.12$, $\Delta\omega = 0.7\gamma$ and 71 elements corresponding to a cutoff frequency of $N\Delta\omega = 6\text{Hz}$. The memory function maintains a value above 0.99 up to a delay of 55.5. The kernel is calculated from the analytical solution of the network and fitted weights. This figure shows that the LRC reservoir takes advantage of its Fourier modes to construct a sinc approximation to the δ function. The bottom panel displays the resulting reconstruction at $\tau = 20$. For this delay, the reconstruction obeys $m(\tau) = 0.9983$.

periods, we used the exact representation of the system trajectory to simulate the reservoir. The long-time limit solution of the reservoir is given by

$$\begin{bmatrix} q(t) \\ \dot{q}(t) \end{bmatrix} = \frac{1}{l(\lambda_+ - \lambda_-)} \begin{bmatrix} 1 & 1 \\ \lambda_+ & \lambda_- \end{bmatrix} \begin{bmatrix} \int_0^\infty d\tau e^{\lambda_+\tau} u(t-\tau) \\ -\int_0^\infty d\tau e^{\lambda_-\tau} u(t-\tau) \end{bmatrix} \quad (11)$$

where $\lambda_\pm = -\frac{\tau}{2l} \pm i\sqrt{\frac{1}{lc} - \frac{\tau^2}{4l^2}} = -\gamma \pm i\omega$. Simply integrating this is computationally inconvenient as it requires the evaluation of the integral over the full timecourse for every timestep. To avoid this we first consider the top integral in eqn. (11). Transforming the integral and using that $u(t) = 0$ for $t < 0$ (the system is not driven before $t = 0$), we have

$$\begin{aligned} f_+(t) &= \int_0^\infty d\tau e^{\lambda_+\tau} u(t-\tau) \\ &= \int_0^t d\tau e^{\lambda_+(t-\tau)} u(\tau). \end{aligned} \quad (12)$$

The second integral may be recovered from this as $f_-(t) = \Re[f_+(t)] - i\Im[f_+(t)]$. The function $f_+(t)$ then obeys the recursion relation for a timestep Δt ,

$$f_+(t + \Delta t) = e^{\lambda_+ \Delta t} (f_+(t) + \int_0^{\Delta t} d\tau e^{-\lambda_+ \tau} u(t + \tau)). \quad (13)$$

which allows for an exact calculation of the trajectory with a single integral and integration over the interval $[0, 5000]$ with a timestep of $\Delta t = 0.05$. After training, the resulting weights were used to estimate the kernel in figure 2 from eqn. (10). Integration was performed using scipy's quadrature package.

B. Quadratic Capacity Figure

The LRC network was the same as that described above. Memristors used had $\alpha = 3$, $\beta = 3$, $\chi = 0.8$. Memristor integrations were done using forward Euler method with a stepsize $\Delta t = 0.02$ on eqn. (17) in the main text. For single or paired memristors, $\Omega_A = I$, $\alpha = 3$, $\beta = 3$ and $\chi = 0.8$. Paired memristors use one element subject to $+u(t)$ and the other subject to $-u(t)$. In all memristor simulations hard boundaries are imposed on the integration to maintain $w \in [0, 1]$. The memristor network consisted of a 5×5 triangular lattice with 56 memristor-voltage generator edges. Each voltage generator was weighted with weights distributed evenly on the set $[-1, -0.1] \cup [0.1, 1]$.

C. Hybrid Network Figure

The top panel of figure 4 in the main text shows a reservoir composed of two memristors driven with opposite polarity, used to drive an LRC network of 10 elements. The memristors were configured and simulated as described in the above section. The trajectory of each memristor, $x_{\pm}(t)$ was used to drive an independent LRC reservoir with $\gamma = 0.4$, $\Delta\omega = 0.4$, and $N = 10$ corresponding to a cutoff frequency of 4 Hz. Each LRC reservoir generated 20 trajectories of the form $q_{n\pm}, \dot{q}_{n\pm}$ for $n = 1 \dots 10$. Memristor trajectories were calculated using forward Euler with a timestep of $\Delta t = 0.02$ and eqn. (17) in the main text.

For the LRC to Memristor reservoir, first the trajectories of an LRC network of 10 circuits as described above were calculated using the driving signal on the interval $[0, 5000]$. From the LRC trajectories $\vec{x}_s = [\vec{q}, \dot{\vec{q}}]$ we define a coupling matrix to the deep memristor layer, $\vec{s}_d = C\vec{x}_s$ such that every sum and difference of trajectories in \vec{x}_s is used to drive an independent memristor pair. As such, for every $i, j \in \{1 \dots 10\}$ there are $k_1 \dots k_4$ such that

$$\begin{aligned} s_{d,k_1} &= x_{s,i} + x_{s,j}, & s_{d,k_2} &= -s_{d,k_1} \\ s_{d,k_3} &= x_{s,i} - x_{s,j}, & s_{d,k_4} &= -s_{d,k_3} \end{aligned}$$

Each of these voltage generators drives a memristor with $\alpha = 3$, $\beta = 3$, $\chi = 0.8$. The reservoir thus contains $2 * 20 * 19$ memristors and generates 20 LRC trajectories giving 780 independent trajectories. As this reservoir contains an LRC network at its surface layer, it also has excellent linear computation capacities, maintaining a computational capacity greater than 0.99 to a delay of $\tau = 10$.

D. Linear and Quadratic Memory Scaling

To estimate the memory capacity of LRC networks with system size, networks were generated with $N = 10, \dots 18$ subcircuits. For each reservoir, the cutoff frequency was chosen as 4 Hz, the frequency resolution as $\Delta\omega = 4/N$, and $\gamma = \Delta\omega$. The resulting reservoirs were driven with an input sequence on $[0, 5000]$. Training was then performed to reconstruct the delayed input $u(t - \tau)$. To evaluate τ_{ϵ} , a bijective search was performed to evaluate the delay at which the memory function $m(\tau) = C_T[u(t - \tau)]$ fell below the threshold $1 - \epsilon$, terminating with a tolerance of 1. Finite size scaling analysis was found to be unnecessary as the calculated capacities did not vary with the length of the training interval. Error estimates are from the termination criteria of the bijective search.

To estimate the quadratic memory capacity $\tau_{\epsilon}^{(2)}$, the trajectories of the LRC reservoirs above were used to drive deep memristor networks as described in the hybrid reservoir section of the main text. To evaluate $\tau_{\epsilon}^{(2)}$, we wish to find the area over which $m_2(\tau_1, \tau_2) > 1 - \epsilon$. First a bijective search was run along the diagonal to find the delay τ^* at which the quadratic memory function $m(\tau, \tau)$ fell below $1 - \epsilon$. Then the function was integrated numerically over $\tau_1 \in [0, 2\tau^*]$ $\tau_2 \in [0, 2\tau^*]$ with subdivisions of 0.5. This provides an uncertainty in the numerical integration on the order of $e_{int} = 2 \cdot 0.5^2 \sqrt{\tau_{\epsilon}^{(2)}}$.

The quadratic capacities $\tau_{\epsilon}^{(2)}$ show clear tendencies towards overestimation for smaller training intervals and larger reservoir sizes. To combat this, we employed a finite size scaling analysis to estimate the capacity $\tau_{\epsilon}^{(2)}$ in the limit of an infinite training interval. A figure demonstrating this analysis is included in the supporting information. We also note that linear and nonlinear memory functions were found to decrease rapidly outside of a region of support. As a consequence, capacities $\tau_{\epsilon}^{(n)}$ depend only weakly on ϵ . However, for small values of ϵ fluctuations play a larger role and make capacities difficult to estimate numerically. We found $\epsilon = 0.1$ struck a reasonable balance between high capacities and low fluctuations on estimates. Errors from the fit are estimated through the elements of the covariance matrix as $e_{fit} = \sqrt{cov_{ii}}$ where i is the index of the constant constant fitting parameter. The total error estimate is given as $e_{tot} = \sqrt{e_{int}^2 + e_{fit}^2}$.

E. Comparison to Echo State Networks

For all tested reservoirs, trajectories were generated on $[0, 5000]$ with training performed on $[100, 4000]$ giving a training error estimate of the nMSE. To assess the generalization error, the weights from the previous training were used to reconstruct the output on $[4000, 5000]$ and a generalization nMSE was calculated as,

$$\text{Gen. nMSE} := \frac{\langle (z(t) - \hat{z}(t)) \rangle_T}{\langle z^2(t) \rangle_T} \quad (14)$$

where the average $\langle \cdot \rangle_T$ is performed over the generalization window $[4000, 5000]$. Note that, unlike the nMSE, this quantity is not constrained to fall within $[0, 1]$.

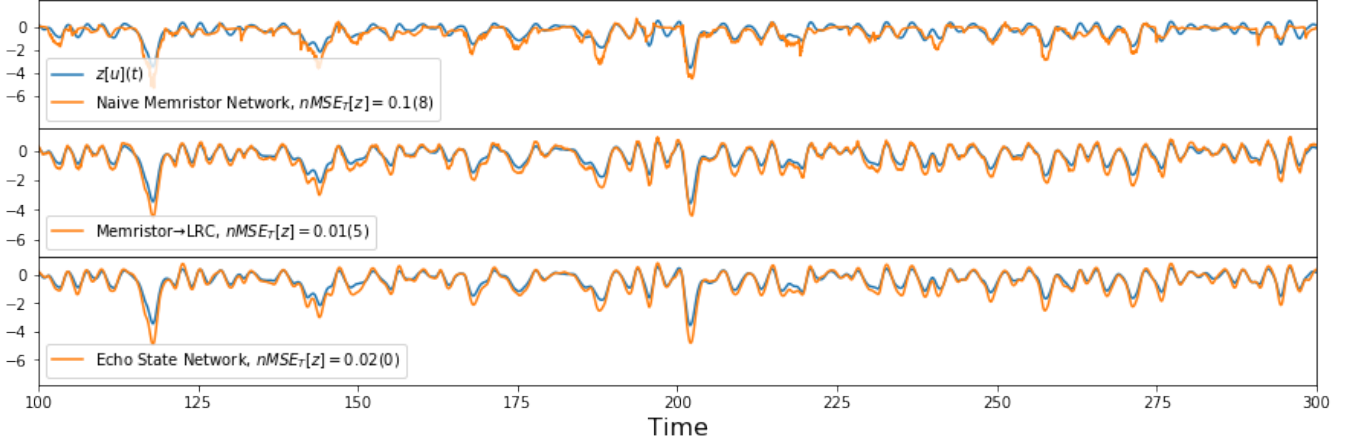


Figure 3. A comparison between memristor, hybrid and echo state network reservoirs on the fitting task described in eqns. (20-22) of the main text. In the top panel, we show the results of a ‘naive’ implementation of a memristor reservoir consisting of a triangular lattice of 800 memristors. In the middle panel we show the results from the hybrid LRC→Memristor reservoir with a total of 780 trajectories. In the bottom panel, we show an echo state network implementation contains 780 elements with parameters tuned to the fitting task. In the legends note that the hybrid networks have a 12-fold improvement over the memristor network alone, perform on par with the ESN implementation.

For the ‘naive’ memristor network implementation, parameters were taken as $\alpha = 3$, $\beta = 1$, $\chi = 0.8$ with inputs weighted on the set $[-1, -0.1] \cup [0.1, 1]$. The network graph was chosen as a 17×17 triangular lattice with 800 edges. Input weights were generated as 400 evenly spaced weights on $[0.1, 1]$, another 400 on $[-1, -0.1]$.

The hybrid LRC→Memristor reservoir was implemented identically as above.

The ESN reservoir obeyed the differential equation

$$\dot{\vec{x}} = -\vec{x} + \tanh(\Omega\vec{x} + \vec{r}_b + \vec{r}_i u(t)) \quad (15)$$

where Ω is a generic matrix of interaction weights between neurons, \vec{r}_b is a bias vector and \vec{r}_i is a vector of input weights. In our case, Ω was chosen to be sparse with a constant fanout of 10, and each weight was initially chosen randomly as ± 1 . After generating this matrix it was scaled to obtain a maximum spectral radius of $r = 0.95$ which was found to give best performance on the fitting task. The bias and input weights were selected uniformly on $[-1, 1]$ and were each independently scaled. Both had a range of acceptable performance centered around 0.2 for the bias weight scaling and 0.1 for the input weight scaling with nMSE ranging from 0.020 to 0.023. Integration was performed with forward Euler on the interval $[0, 5000]$ with a timestep of $\Delta t = 0.05$.

V. PROOF OF COMPUTATIONAL CAPACITY BOUND

Theorem 1 Given a set of n orthonormal functions $\{z_i\}_{i=1}^n$ and a reservoir with capacities $C_T[z_i] \geq 1 - \epsilon$, any function of the form $z = \sum_{i=1}^n a_i z_i$ will have a capacity which is at least $C_T[Z] \geq 1 - n\epsilon$.

We consider a set of n orthonormal functions $\langle z_i z_j \rangle_T = \delta_{ij}$, and a reservoir such that $C_T[z_i] \geq 1 - \epsilon$. The estimate of the reservoir is the projection of the function z_i onto the span of the reservoir trajectories \vec{x} . We write this as $P_X z_i = \hat{z}_i$ and $z_i = \hat{z}_i + e_i$ with $\langle z_i e_j \rangle = 0$ for all i, j . As $C_T[z_i] = 1 - \text{nMSE}[z_i]$ we have

$$\text{nMSE}[z_i] = \frac{\langle (z_i - \hat{z}_i)^2 \rangle}{\langle z_i^2 \rangle} = \langle e_i^2 \rangle = \epsilon_i \leq \epsilon \quad (16)$$

where we have defined ϵ_i as the nMSE of z_i .

We consider a superposition $z = \sum_i a_i z_i$. The estimate of the reservoir will be $\hat{z} = P_x z = \sum_i a_i \hat{z}_i$. As such,

$$\begin{aligned} \frac{\langle (z - \hat{z})^2 \rangle}{\langle z^2 \rangle} &= \frac{\langle (\sum_i a_i e_i)^2 \rangle}{\sum_i a_i^2} \\ &= \frac{\sum_i a_i^2 \epsilon_i + \sum'_{ij} a_i a_j \langle e_i e_j \rangle}{\sum_i a_i^2} \\ &\leq \epsilon + \frac{\sum'_{ij} a_i a_j \langle e_i e_j \rangle}{\sum_i a_i^2} \\ &\leq \epsilon + \frac{\sum'_{ij} |a_i a_j| |\langle e_i e_j \rangle|}{\sum_i a_i^2}. \end{aligned}$$

from Cauchy-Schwarz we have $\langle e_i e_j \rangle \leq \sqrt{\epsilon_i \epsilon_j} \leq \epsilon$. Considering

$$\begin{aligned} \sum'_{ij} (|a_i| - |a_j|)^2 &= \sum'_{ij} a_i^2 - 2|a_i a_j| + a_j^2 \\ &= 2(n-1) \sum_i a_i^2 - 2 \sum'_{ij} |a_i a_j| \geq 0 \end{aligned}$$

from which we find

$$n-1 \geq \frac{\sum'_{ij} |a_i a_j|}{\sum_i a_i^2}. \quad (17)$$

Assembling these we have,

$$1 - C_T[z] = \frac{\langle (z - \hat{z})^2 \rangle}{\langle z^2 \rangle} \leq n\epsilon. \quad (18)$$

This is less pessimistic than it might seem as we were free to choose any basis for z and this corresponds to the worst choice of basis. To see this, consider the subspace of functions as Z . If we take only normalized functions from Z , then these lie on a sphere we will call S_Z . The nMSE is a continuous function from the compact space S_Z to the reals and so attains a maximum. Assume one function that attains this maximum is z^* with $\text{nMSE}[z^*] = \epsilon$. If this is within our basis, then for any normalized function z we approximate we have $\text{nMSE}[z] \leq \epsilon$. The factor of n in eqn. (18) accounts for choosing a basis that overlaps as little as possible with z^* .

We can explicitly construct the maximum error function of the form $z = \sum_i a_i z_i$ with $\langle z^2 \rangle = 1$ by maximizing

$$\max_{\vec{a}, \lambda} \left(\sum_i a_i e_i \right) - \lambda \left(\sum_i a_i^2 - 1 \right) \quad (19)$$

where the normalization constraint has been included through a Lagrange multiplier. The sign is chosen so that λ coincides with the maximal eigenvalue below. Defining a matrix E with columns formed by the error vectors $E = [e_1, e_2, \dots, e_n]$, the maximum error function z has coefficients $\vec{a} = (a_1, \dots, a_n)$ that are the solution of the eigenvalue problem

$$E^T E \vec{a} = \lambda \vec{a} \quad (20)$$

for the maximal eigenvalue λ and normalized eigenvector \vec{a} . In the case where the errors are orthogonal, we have $E^T E = \text{diag}((\epsilon_1, \epsilon_2, \dots, \epsilon_n))$ and the maximal error function z is the basis vector with maximal nMSE.

VI. FEASIBILITY PROPERTIES OF LRC RESERVOIRS

We first consider a single subcircuit. An LRC circuit with component values l, r , and c can be cast as the linear system,

$$\dot{\vec{x}} = \begin{bmatrix} 0 & 1 \\ -\frac{1}{lc} & -\frac{r}{l} \end{bmatrix} \vec{x} + \begin{bmatrix} 0 \\ \frac{s(t)}{l} \end{bmatrix} = A\vec{x} + \vec{u}. \quad (21)$$

where A has eigenvalues $\lambda_{\pm} = -\frac{r}{2l} \pm i\sqrt{\frac{1}{lc} - \frac{r^2}{4l^2}} = -\gamma \pm i\omega$ with negative real part. This procedure generalizes directly to a network of motifs.

For a directed graph \mathcal{G} , define i_e as the current in the direction of an edge e and v_e as the increase in voltage along the edge. We replace each edge with a 2-port circuit called a motif. For the LRC circuit, consider a motif on edge e with two parallel branches containing (a) a voltage generator s_e and resistor r_e in series and (b) a capacitor c_e and inductor l_e in series. The current in the edge i_e and voltage v_e can be written

$$i_e = i_{e,a} + i_{e,b} \quad (22)$$

$$v_e = s_e - r_e i_{e,a} = -\frac{q_e}{c_e} - l_e \frac{di_{e,b}}{dt}. \quad (23)$$

Here $i_{e,a/b}$ is the current through each branch and q_e is the charge on the capacitor. Defining diagonal matrices, $R = \text{diag}([r_e])$, $C = \text{diag}([c_e])$ and $L = \text{diag}([l_e])$ the equations can be written in the vectorial form,

$$\vec{i} = \vec{i}_a + \vec{i}_b \quad (24)$$

$$\vec{v} = \vec{s} - R\vec{i}_a = -C^{-1}\vec{q} - L\frac{d\vec{i}_b}{dt}. \quad (25)$$

We construct a graph divergence operator $B = [s_{n,e}]$ with dimensions $\# \text{ nodes} \times \# \text{ edges}$. For an edge e , $s_{n,e} = 1$ at the node n that the edge enters and $s_{n,e} = -1$ at the node n that the edge exits. With this definition, for a current configuration satisfying Kirchoff's laws we have $B\vec{i} = 0$, and we can write any voltage configuration as $\vec{v} = B^T\vec{p}$ where p_n is a potential at each node. Using these, and that $\vec{i}_b = \frac{d\vec{q}}{dt}$ we can write the first voltage relation as

$$(BR^{-1}B^T)\vec{p} = BR^{-1}\vec{s} + B\frac{d\vec{q}}{dt}. \quad (26)$$

Defining the non-orthogonal projector $\Omega_{B/R^{-1}} = B^T(BR^{-1}B^T)^{-1}BR^{-1}$ we can regain the voltage as,

$$\vec{v} = \Omega_{B/R^{-1}}\vec{s} + \Omega_{B/R^{-1}}R\frac{d\vec{q}}{dt}. \quad (27)$$

Setting this equal to the second voltage expression, we obtain a closed second order ODE for \vec{q} that can be expressed as the linear system,

$$\begin{bmatrix} \ddot{\vec{q}} \\ \dot{\vec{q}} \end{bmatrix} = \begin{bmatrix} 0 & I \\ -(CL)^{-1} & -L^{-1}\Omega_{B/R^{-1}}R \end{bmatrix} \begin{bmatrix} \vec{q} \\ \dot{\vec{q}} \end{bmatrix} + \begin{bmatrix} 0 \\ -L^{-1}\Omega_{B/R^{-1}}\vec{s} \end{bmatrix}. \quad (28)$$

The eigenvalue equation of this system,

$$\lambda \begin{bmatrix} \vec{a} \\ \vec{b} \end{bmatrix} = \begin{bmatrix} 0 & I \\ -(CL)^{-1} & -L^{-1}\Omega_{B/R^{-1}}R \end{bmatrix} \begin{bmatrix} \vec{a} \\ \vec{b} \end{bmatrix} \quad (29)$$

can be written as the quadratic

$$\lambda^2\vec{a} + \lambda L^{-1}\Omega_{B/R^{-1}}R\vec{a} + (RLC)^{-1}\vec{a} = 0. \quad (30)$$

Attempting a solution of the form $\vec{a} = R^{-1}B^T\vec{p}$ gives,

$$\left[\lambda^2 R^{-1} + \lambda L^{-1} + (RLC)^{-1} \right] B^T \vec{p} = 0 \quad (31)$$

which will have a solution when the matrix in brackets is singular. All matrices in this equation are now diagonal, and so this gives n 2nd order equations for the eigenvalues, giving the full set of $2n$ eigenvalues of the original equation,

$$\lambda_{e,\pm} = -\frac{r_e}{2l_e} \pm i\sqrt{\frac{1}{l_e c_e} - \frac{r_e^2}{4l_e^2}}. \quad (32)$$

Despite the fact that the circuits are now connected and can share currents, we find that this does not alter the dynamics at all and a circuit composed of these motifs is equivalent to a collection of separate subcircuits. This motivates our consideration of reservoirs of separate subcircuits in the main text. We also note that independent of the manner of connection, all eigenvalues have negative real parts.

A. Fading Memory

We first establish that reservoirs composed of LRC motifs satisfy the fading-memory property, namely that two identical reservoirs begun in states x_0 and x'_0 and subject to the same driving signal $\vec{u}(t)$ will converge to the same state, $\lim_{t \rightarrow \infty} \eta(t) - x'(t) = 0$.

For $\Delta\vec{x} = \vec{x} - \vec{x}'$

$$\frac{d}{dt}\Delta\vec{x} = A\Delta\vec{x} \quad (33)$$

with solution

$$\Delta\vec{x}(t) = e^{At}\Delta\vec{x}(0). \quad (34)$$

As the eigenvalues of A have negative real part $-\frac{\gamma}{2l}$, the difference between the trajectories will converge to 0 as $e^{-\frac{\gamma}{2l}t}$.

B. State Separation

The equation of motion above for two reservoirs subject to driving signals $\vec{u}(t)$ and $\vec{u}'(t)$ with $\Delta\vec{u}(t) = \vec{u}(t) - \vec{u}'(t)$ leads to the equation of motion,

$$\frac{d}{dt}\Delta\vec{x} = A\Delta\vec{x} + \Delta\vec{u}(t). \quad (35)$$

Two reservoirs begun in the same state $\Delta\vec{x}(0) = 0$ will thus be initially diverging at a rate proportional to the difference between their respective driving signals. In the long time limit, the difference between trajectories can be solved explicitly as,

$$\Delta\vec{x}(t) = \int_0^\infty d\tau e^{A\tau} \Delta\vec{u}(t - \tau). \quad (36)$$

The difference between the two reservoirs is thus identical to a reservoir driven with the difference of the inputs.

VII. FEASIBILITY PROPERTIES OF MEMRISTOR RESERVOIRS

We consider a reservoir composed of memristors, and where the single memristor, idealized as a switch between two resistance values $R_{\text{off}} > R_{\text{on}}$, is described by a parameter $0 \leq \eta_i \leq 1$

$$\frac{d}{dt}\eta_i(t) = -\alpha\eta_i(t) + \frac{I_i(t)}{\beta} \quad (37)$$

where $I_i(t)$ is the current in the device, with a resistance of the device is given by $R(\eta) = R_{\text{off}}(1 - \eta(t)) + R_{\text{on}}\eta(t)$; α and β are phenomenological parameters setting the decay and excitation of the device. It is convenient to write the equation in terms of the parameter $\chi = \frac{R_{\text{off}} - R_{\text{on}}}{R_{\text{off}}}$, which is naturally less than one if $R_{\text{off}} > R_{\text{on}}$.

A memristor network is a model for a general circuit composed of memristors and with voltage generators in series to the memristors, given by the following vectorial and nonlinear differential equation [1]:

$$\frac{d\vec{\eta}}{dt} = -\alpha\vec{\eta}(t) + \frac{1}{\beta}(I - \chi\Omega_A H(t))^{-1}\vec{S} \quad (38)$$

while we do not go into the detail of the derivation of the equation, we point out that Ω_A is a projector operator on the cycle space of the circuit, e.g. $\Omega^2 = \Omega$, while $H_{ij} = \delta_{ij}\eta_i(t)$.

The input to the network can be voltages in series to the memristors, injected at the nodes, or current sources in parallel or injected at the nodes. For all these cases, we have respectively

$$\vec{S} = \begin{cases} \Omega_A \vec{s} & \text{Voltage sources in series} \\ A(A^T A)^{-1} \vec{s}_{ext} & \text{Voltage sources at nodes} \\ \Omega_B \vec{j} & \text{Current sources in parallel} \\ B^T (B B^T)^{-1} \vec{j}_{ext} & \text{Current sources at nodes.} \end{cases}$$

While in the paper we focus on the voltages in series, and thus $\vec{S} = \Omega_A \vec{s}$, the proof below is general. Given the equation above, we now prove some of the key properties for the dynamical system to be feasible as a Reservoir, assuming that we read-out either the voltage or the current in the device.

A. Fading Memory

Consider two network states $\vec{\eta}$ and $\vec{\eta}'$. We will show that any two trajectories will converge if driven by the same source \vec{S} . The squared norm of the difference $\Delta\eta = \vec{\eta} - \vec{\eta}'$ will obey

$$\frac{d}{dt} \|\Delta\vec{\eta}\|_2^2 = \Delta\vec{\eta}^T \frac{d\vec{\eta}}{dt} = 2 \left[-\alpha \|\Delta\vec{\eta}\|_2^2 + \frac{1}{\beta} \Delta\vec{\eta}^T [g(H) - g(H')] \vec{S} \right] \quad (39)$$

calling $g(H) = (1 - \chi\Omega_A H)^{-1}$. Using the identity $(1 - A)^{-1} - (1 - B)^{-1} = (1 - A)^{-1}(A - B)(1 - B)^{-1}$ we have (defining $\Delta H = H - H'$),

$$\frac{d}{dt} \|\Delta\vec{\eta}\|_2^2 = -2\alpha \|\Delta\vec{\eta}\|_2^2 + \frac{2}{\beta} \Delta\vec{\eta}^T [g(H)\chi\Omega_A \Delta H g(H')] \vec{S} \quad (40)$$

$$\leq -2\alpha \|\Delta\vec{\eta}\|_2^2 + \frac{2}{\beta} \|\Delta\vec{\eta}^T [g(H)\chi\Omega_A \Delta H g(H')] \vec{S}\|_2 \quad (41)$$

$$\leq -2\alpha \|\Delta\vec{\eta}\|_2^2 + \frac{2\chi}{\beta} \|\Delta\vec{\eta}\|_2 \|g(H)\chi\Omega_A \Delta H g(H')\|_{sup} \|\vec{S}\|_2 \quad (42)$$

The supremum norm of the matrix can be broken up, $\|g(H)\chi\Omega_A \Delta H g(H')\| \leq \|g(H)\| \|\chi\Omega_A \Delta H\| \|g(H')\|$ and then each part dealt with. The resolvents $g(H)$ will satisfy

$$\|(1 - \chi\Omega_A H)^{-1}\| \leq \frac{1}{1 - \chi\|\Omega_A H\|} \leq \frac{1}{1 - \chi}. \quad (43)$$

where $\|\Omega_A H\| = \bar{\sigma}(\Omega_A H)$. The last part follows as H is a diagonal matrix with all elements in $[0, 1]$ and Ω_A is a projection matrix. Similarly, the middle term,

$$\|\chi\Omega_A \Delta H\| \leq \chi \|\Omega_A\| \|\Delta H\| \leq \chi \|\Delta\vec{\eta}\|_2. \quad (44)$$

Assembling these pieces,

$$\frac{d}{dt} \|\Delta\vec{\eta}\|_2^2 \leq \left(-2\alpha + \frac{2\chi}{\beta(1 - \chi)^2} \|\vec{S}\|_2 \right) \|\Delta\vec{\eta}\|_2^2. \quad (45)$$

The distance between the trajectories will be decreasing if

$$\left(-2\alpha + \frac{2\chi}{\beta(1 - \chi)^2} \|\vec{S}\|_2 \right) < 0 \quad \leftrightarrow \quad \|\vec{S}\|_2 < \frac{\alpha\beta(1 - \chi)^2}{\chi}. \quad (46)$$

If we replace the dissipative term in the dynamics $-\alpha\vec{\eta}$ with the more general $-\alpha f(\vec{\eta})$ and require that this satisfy

$$\Delta\vec{\eta}^T (f(\vec{\eta}) - f(\vec{\eta}')) \geq C \|\Delta\eta\|_2^2 \quad (47)$$

then the bound is modified to $\|\vec{S}\|_2 < \frac{C\alpha\beta(1 - \chi)^2}{\chi}$. As long as the system is driven with small enough voltages or currents, a memristor network satisfies the contracting property. If we read-out the resistive states, then the proof ends here, as the resistive states are continuous functions of the internal states. If instead we read out the voltage across the motif, then we need to show that this implies that also the voltage states are the same.

We now have two possibilities. If we input the system with voltage in series with the resistor (or memristor), then this implies that the voltage on the j -th motif is $V_{ro}^j(t) = V_c^j(t) + i_j(t)R_j(\eta(t))$, where V_{ro}^j is the read-out function. In this case, as long as the current is non-zero almost everywhere, then the echo state property is valid. In the case in which the current source is in parallel to the motif, then we have a voltage input function of the form $V_c^j(I_c(t))$ which is not easily related to the voltage source, but the argument is equally valid.

B. State Separation

We demonstrate a local form of state separation: for two memristor networks begun in the same state, $\Delta\vec{\eta} = 0$ but driven with two different sources \vec{S} and \vec{S}' , the trajectories must diverge.

The difference between the two trajectories will obey

$$\dot{\vec{\eta}} = -\alpha\vec{\eta} + \frac{1}{\beta}(I - \chi\Omega_A H)^{-1}\vec{S} - \frac{1}{\beta}(I - \chi\Omega_A H)^{-1}\vec{S}^t \quad (48)$$

which at $\Delta\vec{\eta} = 0$ is

$$\dot{\vec{\eta}} = \frac{1}{\beta}(I - \chi\Omega_A H)^{-1}(\vec{S} - \vec{S}^t). \quad (49)$$

The matrix $(I - \chi\Omega_A H)^{-1}$ has a trivial kernel which can be seen from: (1) that its kernel must be the same as $(I - \chi\Omega_A H)$, and (2) this has the same spectrum as $I - \chi\sqrt{H}\Omega_A\sqrt{H}$. As Ω_A is a projection matrix, the elements of H are in $[0, 1]$ and $0 < \chi < 1$ we have, for normalized \vec{v}

$$\vec{v}^T \sqrt{H}\Omega_A\sqrt{H}\vec{v} \geq \vec{v}^T H\vec{v} = \sum_i v_i^2 \eta_i \leq \sum_i v_i^2 = 1 \quad (50)$$

$$\vec{v}^T (I - \chi\sqrt{H}\Omega_A\sqrt{H})\vec{v} \geq (1 - \chi) > 0 \quad (51)$$

Now, if the voltage or the current sources are at the nodes, it is true that for sufficiently small (different) inputs \vec{S}_{ext} and \vec{j}_{ext} the state separation cannot be always preserved. This is due to the fact that the operators $A(A^T A)^{-1}$ and $B^T(BB^T)^{-1}$ can have non-trivial kernels. The reason can be easily seen if the memristor network is input-led via voltage sources in series or currents in parallels, there can be redundancy in the input. In fact, if

$$\begin{aligned} \vec{j}_{ext}^1 &= \vec{j}_{ext}^2 + (I - \Omega_B)\vec{k} \\ \vec{S}_{ext,1} &= \vec{S}_{ext,2} + (I - \Omega_A)\vec{k} \end{aligned} \quad (52)$$

for arbitrary \vec{k} , we will have $\vec{S}_1 - \vec{S}_2 = 0$ identically. We can thus construct simple counterexamples for which the state evolution is identical for completely different inputs, and violates the state separation property. This is due to a freedom in defining the voltage drops on the edge, and is reflected in how we can input the system. This property has been described in previous papers. Thus, state separation is true as long as different inputs are not equal up to the transformation described in eqn. (52).

VIII. SOLUTION OF LRC CIRCUITS

An LRC circuit has the long time limit solution,

$$\begin{bmatrix} q(t) \\ \dot{q}(t) \end{bmatrix} = \frac{1}{l(\lambda_+ - \lambda_-)} \begin{bmatrix} 1 & 1 \\ \lambda_+ & \lambda_- \end{bmatrix} \begin{bmatrix} \int_0^\infty d\tau e^{\lambda_+\tau} u(t - \tau) \\ -\int_0^\infty d\tau e^{\lambda_-\tau} u(t - \tau) \end{bmatrix} \quad (53)$$

where $\lambda_\pm = -\frac{r}{2l} \pm i\sqrt{\frac{1}{lc} - \frac{r^2}{4l^2}} = -\gamma \pm i\omega$.

Given a γ and $\Delta\omega$, we choose $l_n = 1$, $r_n = 2\gamma$ and

$$c_n = \frac{1}{n^2 \Delta\omega^2 + \gamma^2} \quad (54)$$

in which case we have that the resulting LRC circuits have eigenvalues $\lambda_{n,\pm} = -\gamma \pm in\Delta\omega$. The resulting trajectories of the system are

$$\begin{aligned} q_n(t) &= \frac{1}{ln\Delta\omega} \int_0^\infty d\tau e^{-\gamma\tau} \sin(n\Delta\omega\tau) u(t - \tau) \\ \dot{q}_n(t) &= \frac{1}{ln\Delta\omega} \int_0^\infty d\tau e^{-\gamma\tau} [n\Delta\omega \cos(n\Delta\omega\tau) - \\ &\quad \gamma \sin(n\Delta\omega\tau)] u(t - \tau). \end{aligned} \quad (55)$$

As noted in the main text, a linear transformation of these trajectories can be expressed in a form that resemble the familiar Fourier transform.

$$x_n(t) = \int_0^\infty d\tau e^{-\gamma\tau} \sin(n\Delta\omega\tau)u(t-\tau) \quad (56)$$

$$y_n(t) = \int_0^\infty d\tau e^{-\gamma\tau} \cos(n\Delta\omega\tau)u(t-\tau). \quad (57)$$

The set of frequencies ranging from $\Delta\omega$ to $N\Delta\omega$ set the bandwidth of signals that the network can reconstruct, while γ imposes a cutoff time. In order for the network to perform reconstructions, this should suppress the input outside of an interval given by the lowest frequency $\Delta\omega \sim \frac{1}{\tau}$. We thus choose $\gamma = \tau$ in our construction of LRC networks.

IX. VOLTERRA SERIES SOLUTION OF MEMRISTOR EQUATIONS

For a single memristor we can use the expansion of the inverse and integrate out the linear term to write the equation as

$$\frac{d}{dt}(e^{\alpha t}x) = \frac{1}{\beta}e^{\alpha t} \sum_{n=0}^{\infty} (\chi x)^n u(t). \quad (58)$$

Then integrating and taking the long time limit, we have a formal expression for x as,

$$\eta(t) = \frac{1}{\beta} \sum_{n=0}^{\infty} \chi^n \int_0^\infty d\tau e^{-\alpha\tau} x^n(t-\tau)u(t-\tau). \quad (59)$$

We assume a solution in the form of a Volterra series expansion,

$$\begin{aligned} \eta(t) &= h_0 + \int_0^\infty d\tau_1 h_1(\tau_1)u(t-\tau_1) \\ &+ \int_0^\infty d\tau_1 d\tau_2 h_2(\tau_1, \tau_2)u(t-\tau_1)u(t-\tau_2) + \dots \end{aligned} \quad (60)$$

$$= h_0 + \sum_{n=0}^{\infty} H_n u. \quad (61)$$

Inserting this into eqn. (59) and matching powers of u we have

$$h_0 = 0 \quad (62)$$

$$H_1 u = \frac{1}{\beta} \int_0^\infty d\tau_1 e^{-\alpha\tau_1} u(t-\tau_1) \quad (63)$$

$$H_2 u = \frac{\chi}{\beta^2} \int_0^\infty d\tau_1 \int_{\tau_1}^\infty d\tau_2 e^{-\alpha\tau_2} u(t-\tau_1)u(t-\tau_2) \quad (64)$$

with subsequent powers following similarly. We immediately observe that: the nonlinear kernels produced by memristors are moderated by powers of $0 \leq \chi \leq 1$, and the kernels take the form of low pass filters of products of the input signal, decaying at a rate governed by α .

For the case of networks of memristor elements, the same manipulations lead to a formal expression for $\eta(t)$ which includes the effect of interactions through the cycle space projector Ω . When the network is driven on each edge by a source \vec{u} ,

$$\eta(t) = \frac{1}{\beta} \sum_{n=0}^{\infty} \chi^n \int_0^\infty d\tau e^{-\alpha\tau} (\Omega X(t-\tau))^n \Omega \vec{u}(t-\tau). \quad (65)$$

This leads to corresponding terms in the expansion

$$h_0 = 0 \quad (66)$$

$$H_1 \vec{u} = \frac{1}{\beta} \int_0^\infty d\tau_1 e^{-\alpha\tau_1} \Omega \vec{u}(t-\tau_1) \quad (67)$$

$$H_2 \vec{u} = \frac{\chi}{\beta^2} \int_0^\infty d\tau_1 \int_{\tau_1}^\infty d\tau_2 e^{-\alpha\tau_2} \Omega U(t-\tau_1) \Omega \vec{u}(t-\tau_2) \quad (68)$$

where we have used the convention $U = \text{diag}(\vec{u})$.

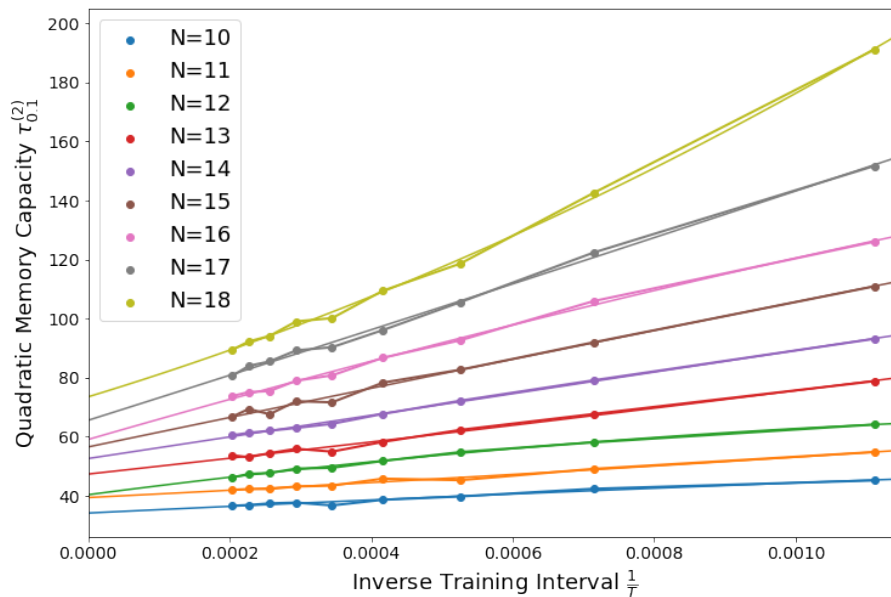


Figure 4. The finite size scaling analysis of quadratic memory capacities in hybrid LRC→Memristor reservoirs. Estimates from simulations are shown by circular markers connected by thick lines. Sizes in the legend are that of the surface LRC reservoir (number of subcircuits). A surface LRC reservoir of size N corresponds to $8N^2 - 2N$ total trajectories. Estimates of the quadratic memory capacity are shown as a function of the inverse training time $\frac{1}{T}$. A 2nd-order polynomial fit is also shown at each size. The capacities given in the main text correspond to the values of the fit at $\frac{1}{T} = 0$.

X. FINITE SIZE SCALING OF QUADRATIC MEMORY CAPACITIES

As noted in the main text, the quadratic memory capacities $\tau_{\epsilon}^{(2)}$ show a tendency towards overestimation for finite training intervals. This may be seen clearly in figure 4 where we have plotted the quadratic capacities for various reservoir sizes estimated from simulation against the inverse training time $\frac{1}{T}$. The sizes given in the figure legend correspond to the number of subcircuits in the surface LRC reservoir while the total number of trajectories in each reservoir is $8N^2 - 2N$. For each size, a 2nd-order polynomial fit is also plotted. Fits were performed using Numpy’s polyfit function and the constant parameter was taken as the limiting value as $\frac{1}{T} \rightarrow 0$. These are plotted against reservoir size in the main text, figure 5.

-
- [1] Caravelli, F., Traversa, F. L., and Di Ventra, M. (2017). Complex dynamics of memristive circuits: Analytical results and universal slow relaxation. *Physical Review E*, 95(2):022140.
 - [2] Dambre, J., Verstraeten, D., Schrauwen, B., and Massar, S. (2012). Information processing capacity of dynamical systems. *Scientific reports*, 2:514.
 - [3] Hermans, M. and Schrauwen, B. (2010). Memory in linear recurrent neural networks in continuous time. *Neural Networks*, 23(3):341–355.
 - [4] Inubushi, M. and Yoshimura, K. (2017). Reservoir computing beyond memory-nonlinearity trade-off. *Scientific reports*, 7(1):10199.